Spring 2021

The Effect of the Interaction of Exercise Training and Isolation on the Serotonergic System of App/Ps1 Mice

Bailey J. Dansby
Missouri State University, dansbyb@sedalia200.org

THE EFFECT OF THE INTERACTION OF EXERCISE TRAINING AND ISOLATION ON THE SEROTONERGIC SYSTEM OF APP/PS1 MICE

A Master's Thesis

Presented to

The Graduate College of

Missouri State University

In Partial Fulfillment

Of the Requirements for the Degree

Master of Science, Cell & Molecular Biology

By

Bailey Dansby

May 2021

THE EFFECT OF THE INTERACTION OF EXERCISE TRAINING AND ISOLATION ON THE SEROTONERGIC SYSTEM OF APP/PS1 MICE

Biomedical Sciences

Missouri State University, May 2021

Master of Science

Bailey Dansby

ABSTRACT

Alzheimer's disease (AD) is a complex neurodegenerative disease that is characterized by the deposition of amyloid beta (Aβ) peptides and, consecutively, by a loss of memory and cognitive functions. The amyloid cascade hypothesis suggests that Aβ deposition is the main pathogenic of AD. There is evidence that both changes in production and clearance of Aβ may be involved in AD pathology. Past studies have shown that exercise training leads to an upregulation in proteins directly involved with Aβ clearance. Chronic stress is thought to exacerbate AD pathology by increasing production of Aβ. Studies have also demonstrated a link between serotonin signaling and decreased Aβ production. Although these factors affecting AD pathology have each been investigated, the interplay between all three has yet to be evaluated. This study aimed to examine the effects of chronic stress and exercise training on both Aβ levels, as well as serotonin signaling. APP/PS1 mice were divided into housing and exercise groups: sedentary and isolated, sedentary and socially housed, exercise trained and isolated, and exercise trained and socially housed. Mice were also divided based on sex. Due to the COVID-19 pandemic not all goals of this project were met. The results demonstrate that exercise training may be able to rescue the negative effects of isolation on Aβ deposition; however, a training effect was not produced in the exercise trained groups, so the trends of this research may need to be reevaluated.

KEYWORDS: Alzheimer's disease, exercise training, Aβ, chronic stress, isolation, serotonin

THE EFFECT OF THE INTERACTION OF EXERCISE TRAINING AND ISOLATION ON THE SEROTONERGIC SYSTEM OF APP/PS1 MICE

By

Bailey Dansby

A Master's Thesis
Submitted to the Graduate College
Of Missouri State University
In Partial Fulfillment of the Requirements
For the Degree of Master of Science, Cell & Molecular Biology

May 2021

Approved:

Scott Zimmerman, Ph.D., Thesis Committee Chair

Benjamin Timson, Ph.D., Committee Member

Lyon Hough, Ph.D., Committee Member

Julie Masterson, Ph.D., Dean of the Graduate College

ACKNOWLEDGEMENTS

First and foremost, I would like to express my gratitude for my thesis advisor, Dr. Scott Zimmerman. You pushed me to grow, both personally and academically, in ways I never would have without this experience. I will never be able to express how thankful I am for having met and worked with you. I am also grateful for my other committee members, Dr. Benjamin Timson and Dr. Lyon Hough. Both offered invaluable advice and expertise throughout my project.

I would also like to thank the graduate students who took me in when I was new and showed me what and what not to do: Justin Lawson, Jordan Jensen and Kaylin Dobbs. To the undergraduates who put in hours of work on this project, I will never be able to thank you enough. I want to thank my friends: Hattie, Simone, Keaton and Khaled. They were indispensable throughout this project.

I must thank Dr. John Cirrito and Dr. Carla Yuede allowing me to work in their lab at Washington University to complete my project. The experiences I from my time with you both are irreplaceable, and I will always cherish my time in your lab.

I could not have completed my project without the unwavering support from my family. Thank you, mom and dad, for raising me to persevere and for always being there for me. I also want to extend a huge thank you to my husband, Josh Dansby, for keeping me going and always offering a helping hand.

Finally, I have to thank my lab partner, Lydia Holtmann. Words cannot describe the bond we have formed while working on this project. I'm thankful for all the laughs, late night study sessions, and even all the tears we experienced together for the last couple of years.

TABLE OF CONTENTS

Literature Review	Page 1
Overview of Alzheimer's Disease	Page 1
Aβ Production and Clearance	Page 6
Factors Affecting Alzheimer's Disease Pathology	Page 23
Materials and Methods	Page 32
Experimental Design	Page 32
Tissue Collection and Preparation	Page 34
Protein Analysis	Page 37
Results	Page 42
Standard Curve Practice	Page 42
WT and APP/PS1 Practice Mice	Page 46
Citrate Synthase Analysis	Page 54
Aβ Analysis	Page 55
Discussion	Page 58
Standard Curve Practice	Page 58
WT and APP/PS1 Practice Mice	Page 60
Citrate Synthase Analysis	Page 61
Aβ Analysis	Page 61
Intended Methods	Page 63
Summary, Conclusions and Future Directions	Page 65
References	Page 66
Appendix	Page 95

LIST OF TABLES

Table 1. APP modifications and the effects on localization and Aβ production Page 10

Table 2. Concentrations of Single $A\beta_{40}$ Standard Curve in 5 Duplicate pairs Page 43

Table 3. Analysis of Single $A\beta_{40}$ Standard Curve in 5 Duplicate pairs Page 43

Table 4. Concentrations of $A\beta_{40}$ Standard Practice Curves in Triplicate #1 Page 46

Table 5. Analysis of $A\beta_{40}$ Standard Practice Curves in Triplicate #1 Page 47

Table 6. Concentrations of $A\beta_{40}$ Standard Practice Curves in Triplicate #2 Page 49

Table 7. Analysis of $A\beta_{40}$ Standard Practice Curves in Triplicate #2 Page 50

Table 8. Practice Mouse Tissue Cerebellum Weights Page 52

Table 9. Total Protein Concentrations of APP/WT Mouse Samples Page 54

Table 10. APP/WT Mouse Cerebellum Amyloid Concentrations Page 55

Table 11. APP/WT Mouse Cerebellum Amyloid Analysis Page 56

LIST OF FIGURES

Figure 1. Ages of people with Alzheimer's Disease Page 4

Figure 2. APP structure and enzymatic processing sites Page 7

Figure 3. Pathway of neuronal activity modulation on APP endocytosis Page 14

Figure 4. Summary of APP processing pathways Page 15

Figure 5. Sequential Cleavages of APP by γ-secretase Page 20

Figure 6. Divisions of physical activity Page 24

Figure 7. Experimental design for animal groups Page 32

Figure 8. Experimental timeline Page 33

Figure 9. Loading Pattern of Single $A\beta_{40}$ Standard Curve in 5 Duplicate pairs Page 42

Figure 10. Comparison of Experimental and Calculated Amyloid Standard Concentrations for the Single $A\beta_{40}$ Standard Curve Page 44

Figure 11. Loading Pattern of $A\beta_{40}$ Standard Practice Curves in Triplicate #1 Page 45

Figure 12. Comparison of Experimental and Calculated Amyloid Standard Concentrations of $A\beta_{40}$ Standard Practice Curves in Triplicate #1 Page 48

Figure 13. Loading Pattern of $A\beta_{40}$ Standard Practice Curves in Triplicate #2 Page 49

Figure 14. Comparison of Experimental and Calculated Amyloid Standard Concentrations of $A\beta_{40}$ Standard Practice Curves in Triplicate #2 Page 51

Figure 15. Loading Pattern for PBS, Triton and Guanidine Extracted APP/WT Mouse Samples Page 53

Figure 16. Hippocampal amyloid beta concentrations in social and isolated mice Page 57

Figure 17. Citrate synthase activity in sedentary and exercised groups Page 57

LITERATURE REVIEW

Overview of Alzheimer's Disease

Alzheimer's disease (AD) is a neurodegenerative disease that effects millions in the United States, making it the most prevalent form of dementia. Most common in the elderly, ages 65 and older, AD has hallmark symptoms of memory defectiveness and language impairment. The brain changes associated with AD, that lead to cognitive issues, can begin 20 years prior to noticeable symptoms. There are three stages of AD: preclinical AD, mild cognitive impairment (MCI) and dementia (Jack et al., 2011; Albert et al., 2011; McKhann et al., 2011).

In preclinical AD, no symptoms are present, but brain changes have already begun, such as an increased in the Aβ peptide (Alzheimer's Disease Facts and Figures, 2019). Preclinical AD typically goes unnoticed, as people do not routinely check for upregulation of AD associated biomarkers without cognitive impairment.

For someone suffering from MCI, symptoms of cognitive decline are present and are greater than expected for that person's age range. Although symptoms are present, the change in cognitive function is not detrimental enough to interfere with everyday life. Close to 20% of people over the age of 65 have MCI (Roberts & Knopman, 2013) Five years after MCI diagnosis, 38% of people had developed dementia (Mitchell & Shiri-Feshki, 2009). Considering AD is most common in the elderly population, it can be difficult to distinguish between age-related changes and MCI. For instance, while forgetting names and appointments is pretty common, forgetting the same thing numerous times can be indicative of MCI. Also, excessive reliance on memory aids, like notes or phone apps, can be indicative of MCI. Other common symptoms at this stage include: finding problem solving more difficult, confusion in time or

place, withdrawal from social settings, as well as changes in mood and personality (Alzheimer's Disease Facts and Figures, 2019).

As memory and behavioral symptoms begin to interfere with daily life, and there is clear evidence of brain related changes MCI becomes AD. Symptoms can worsen over time in dementia or change completely. There are three sublevels within AD pathology mild, moderate and severe (Alzheimer's Disease Facts and Figures, 2019). With mild dementia, people typically remain independent, but require help in with certain tasks, like organizing medicine. Normally, people at this stage maintain the ability to participate in their favorite activities, drive and do everyday housework. Once AD progresses into the moderate stage, the ability of the patient to live independently decreases. This stage typically lasts the longest. The ability to communicate tends to decline with moderate dementia due to AD. Specifically, patients may have difficulty bathing and dressing. Patients may also become intermittently incontinent. Late in the progression of moderate dementia, personality and behavioral changes can occur, including suspiciousness of one's caretakers and doctors (Alzheimer's Disease Facts and Figures, 2019). For patients with severe dementia, constant care is typically required, and the patient may even become bed-bound leading to many hardships, including, vulnerability to sepsis and skin infections. It is not uncommon, for these patients to experience some damage in brain regions that control swallowing, increasing the risk for aspiration of food. Aspiration pneumonia is one of the main causes of death associated with AD (Alzheimer's Disease Facts and Figures, 2019).

Diagnosis and Treatment. Alzheimer's disease can be difficult to diagnose. Instead of using AD biomarker testing, due to issues with availability and reliability, many doctors rely on family medical and psychological histories, family input about cognitive function, cognitive tests and physical examinations, and blood tests to rule out other forms of dementia, like certain

vitamin deficiencies. Even after being diagnosed, there is not much help therapeutically for AD. Currently, five drugs are available for the treatment of AD and have been approved by the U.S. Food and Drug Administration (FDA): rivastigmine, donepezil, memantine, galantamine, and a combination of donepezil and memantine (Alzheimer's Disease Facts and Figures, 2019). Like many neuroactive medications, the effectiveness of these drugs varies between people.

Although there are not many drugs on the market to aid those with AD, and no drugs to prevent or cure AD, there are many non-pharmacological tactics that help improve AD symptoms. The main therapies are cognitive stimulation and exercise. Cognitive stimulation has favorable effects on cognition, but did not affect mood, or the ability to perform normal daily activities (reviewed in Aguirre et al., 2013).

Exercise, both aerobic and non-aerobic, has a demonstrated positive effect on cognition, and may also slow the rate of cognitive decline in AD patients. However, there are many variables that make it hard to fully assess exercises effect on AD pathology, including length and intensity of exercise. In mice, downregulation of Aβ have been seen following moderate intensity exercise training regimens (Moore et al., 2016).

Prevalence and Incidence. There are 5.8 million Americans living with AD, and 5.6 million of those are age 65 years or older (Hebert et al., 2013). Age seems to be the biggest risk factor for AD, as 81% of people suffering from dementia due to AD are 75 or older (Figure 1).

Although the number of cases of AD is already extremely high, it is likely not quite high enough due to the obstacles faced during diagnosis. In the coming years, the number of people afflicted by AD will presumably skyrocket, as the number of people age 65 and older, in America, is expected to grow from 55 million now to 88 million in 2050 (He et al., 2016; US Census Bureau, 2014). Although the incidence of AD is debated between studies, normally

somewhere between 500,00 and 910,000 people develop AD in the US per year (Rajan et al., 2019). By 2025, a 12% increase in AD cases throughout the US is expected (Weuve et al., 2015).

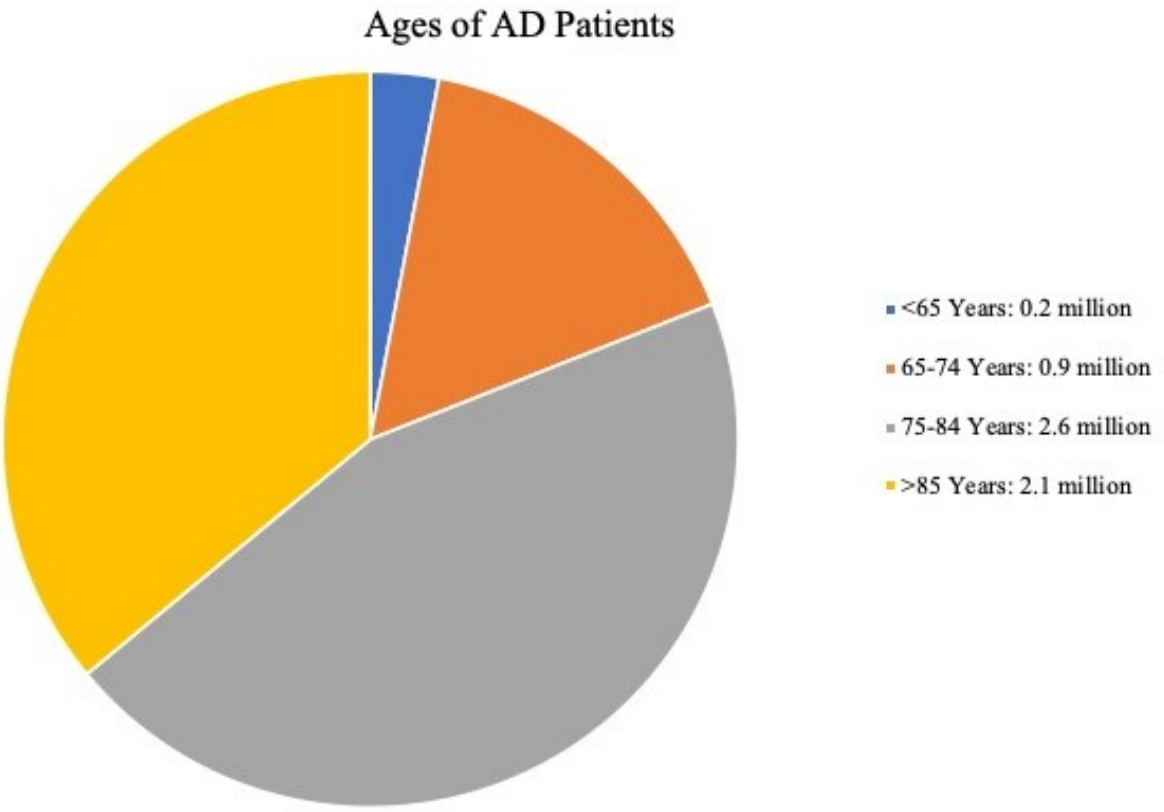

Figure 1. Ages of people with Alzheimer's Disease. (Adapted from Hebert et al., 2013).

Sex Disparities. Two-thirds of Americans afflicted with AD are women (Hebert et al., 2013). There is not sufficient evidence to determine whether this discrepancy between men and women is due to a typically longer life (longevity hypothesis), or due to differences in molecular pathways between the sexes (Carter et al., 2012). The longevity hypothesis proposes that females only seem more affected because on average women live longer than men (Chene et al., 2015; Seshadri et al., 1997; Hebert et al., 2001). Survival bias is also a factor, because only the healthiest men that do live to older ages, reducing the risk for AD development. However, there are variations in mechanisms between men and women when it comes to AD, which could lead

to different risk levels. For example, women respond differently to chronic stressors than men (Yan et al., 2018).

Ethnic Disparities. Racial and ethnic differences appear to play a role in the risk of developing AD. African-Americans are twice as likely to be afflicted compared to Caucasians of the same age (Potter et al., 2009; Gurland et al., 1999). Hispanics are 1.5 times as likely to develop AD compared to Caucasians (Gurland et al., 1999; Haan et al., 2003; Samper-Ternent et al., 2012). However, Asian Americans have the lowest risk of being afflicted (Mayeda et al., 2016). It remains unclear why-these discrepancies are seen. They are often attributed to increased exposure of many minorities to AD risk factors like, poverty, lower levels of education, and increased stress due to adversity and discrimination (Lines et al., 2014; Glymour & Manly, 2008; Zhang et al., 2016).

Deadliness of AD. Being the sixth-leading cause of death, AD was responsible for 121,404 deaths in the 2017 (Heron, 2018; US Department of Health and Human Services, 1999-2017). For those over the age of 65, AD was the fifth-leading cause of death (Heron, 2018). In addition to being a top cause of death, AD is also a leading cause of disability and morbidity. Deaths due to AD might be even higher than currently reported because many deaths are attributed to acute conditions that are actually just a side effect of the underlying AD (Ives et al., 2009; Romero et al., 2014). For example, pneumonia is listed as the cause of death for many afflicted by AD, but, as noted previously, pneumonia may be caused by aspiration of food due to impaired swallowing in AD. Whether it is listed as the cause of death, or is linked to a patient's death, those with AD have significantly increased mortality. Specifically, among 70-year old's, 61% with AD, whereas only 30% of those without AD, are not expected to reach 80 years of age

(Arrighi et al., 2010). As the mean age of the population in America rises, AD is becoming an increasingly common cause of death.

AD is a debilitating disease that effects millions (Alzheimer's Disease Facts and Figures, 2019). At first, AD might be comparable to age related cognitive changes, like increased forgetfulness, but with time, AD patients lose their independence and require continually care. AD is not only detrimental to those afflicted, but also to families and caregivers.

Amyloid Beta Production and Clearance

APP Overview. Amyloid precursor protein (APP) is a member of a type 1 membrane protein family including APLP1 and APLP2 (Wasco et al., 1993). The entire mammalian APP family has a conserved structure including a large ectodomain, a single transmembrane domain and one internal domain (Figure 2).

The ectodomain is responsible for substrate adhesion and seems to have a neurotrophic effect (Small et al., 1994). It has two regions, E1 and E2. E1 is most distal from the membrane, and includes two subunits; the heparin binding domain (HBD) and the copper/metal binding domain. Within the HBD there is a loop compromised of mostly basic amino acids, to which heparin can bind (Small et al., 1994). Heparin is a naturally occurring anticoagulant, and possibly has some anti-inflammatory effects (reviewed in Oduah et al., 2016). The E2 region contains the active component of APP, the amino acid sequence "RERMS", as well as many α-helices that can easily dimerize with other APP proteins (Xue et al., 2011). This indicates that the E2 domain plays a role in self-association of APP, which can aid in cell adhesion and communication, as well as regulate APP processing. The Aβ sequence begins in close proximity to the membrane, and it continues into the transmembrane domain (Figure 2). The APP

intracellular domain (AICD) is highly conserved and important to modulating APP function. The AICD is 47 amino acids in length and contains the "YENPTY" motif which is a C-terminal endocytic signal (Lai et al., 1995). The AICD plays a role in APP localization, metabolism and cell signaling.

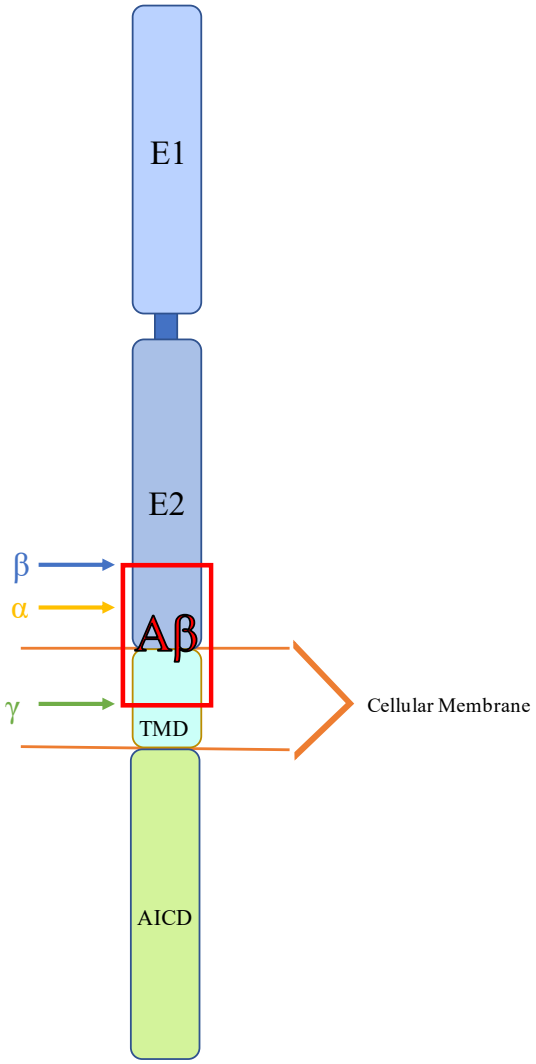

Figure 2. APP structure and enzymatic processing sites.

The APP gene is found on the long arm chromosome 21 and contains 18 exons (Yoshikai et al., 1990). Due to alternative splicing there are numerous isoforms of APP varying from 365 amino acids to 770 aa. The main, Aβ producing, isoforms are APP695, APP751 and APP770.

Certain alternative splicing sites seem to be favored based on the tissue, as APP695 is found almost exclusively in neurons (Kang et al., 1987). APP770 and APP751 are present in astrocytes and microglial cells (Rohan de Silva et al., 1997).

The exact function of APP has not yet been discovered, but there is strong evidence that APP plays a role in many critical biological functions. The APP gene is a housekeeping gene, meaning that it is continuously expressed and required for essential cellular functioning (Salbaum et al., 1988). A number of transcription factors that regulate cell proliferation and mitosis genes also have a regulatory role for APP transcription (Salbaum et al., 1988). This suggests that APP may also have a role in cell growth. This is supported by data demonstrating an increase in APP during times of development and growth (Clarris et al., 1995).

Many studies using APP-KO mice, have demonstrated that mice lacking the APP gene are still viable and fertile, but are smaller in stature, have a reduced overall weight of 15-20%, have a decreased brain weight as well as minor defects in locomotion, gliosis and long-term potentiation (Zheng et al., 1995; Magara et al., 1999). Since APP-KO mice are viable and fertile AP, alone, cannot play a key role in development. However, studies utilizing double knockouts of APP and APLP2 have shown a lethal phenotype, suggesting that there is redundancy in the function of APP and APLP2 (Heber et al., 2000).

The structure of APP resembles that of cell-surface receptors (Kang et al., 1987) and growth factors receptors (Rossjohn et al., 1999). There is a hydrophobic site within the E1 domain that could potential be a protein binding site (Rossjohn et al., 1999). Some data indicate that when heparin is bound, APP dimerizes at that hydrophobic pocket (Gralle et al., 2006). Previously noted, there are additional dimerization spots in the E2 domain of APP. Specifically the E2 region is responsible for antiparallel dimerization (Wang & Ha, 2004). APP can

homodimerize or heterodimerize with APLP1 and APLP2 (Khalifa et al., 2010). Dimerization of APP within the ectodomain can aid in cell to cell adhesion and interaction, but dimerization closer to, or within the membrane seems to regulate APP processing. Although a clearly defined function of APP is not available, it is reasonable to conclude that APP plays a role in growth, regulation, and cell-cell interactions to some extent.

APP mRNA is translated by membrane bound polysomes, and immediately following, the N-terminal peptide signal is removed. The mature APP peptide translocates to the ER where it continues to the Golgi apparatus and trans Golgi network (TGN). Throughout these sites, many posttranslational modifications occur, such as glycosylation, phosphorylation, palmitoylation, ubiquitination and sumoylation (Selkoe, 2001). All of these modifications lead to changes in trafficking of APP, and therefore, secretase co-localization, which can affect Aβ production. From the Golgi and TGN, around 10% of APP reaches the plasma membrane, but most remains in the late stages of the secretory pathway (Choy et al., 2012). There also seems to be a small fraction of APP that goes directly into endosomes from the TGN (Choy et al., 2012). At the cell surface, APP is either rapidly cleaved by α-secretases, or is internalized, due to the a C-terminal endocytic signal within the AICD, via Catherin-mediated endocytosis (Yamazaki et al., 1996). Once internalized, most APP enters the endosomal-lysosomal pathway, but a small fraction of APP either gets recycled back to the cell surface or goes back to the TGN (Haas et al., 1992).

APP Regulation. As APP travels through the secretory pathway, it goes through many posttranslational modifications, many of which effect trafficking of APP, and therefore APP processing (Table 1).

First, as newly translated APP enters the endoplasmic reticulum (ER) it is glycosylated on two residues (Asn467 and Asn496) by oligosacharyl transferase (OST) (Pahlsson et al.,

1992). Once APP passes through to the Golgi apparatus, O-glycosylation occurs on many serine or threonine residues. Both N-glycosylation and O-glycosylation are required for APP trafficking to the plasma membrane (Greenfield et al., 1999). Interestingly, a special type of O-glycosylation, O-GlcNacylation, which consists of adding a β-N-acetylglucosamine (GlcNAc) to serine or threonine residues (Griffith et al., 1995), results in inhibition endocytosis of APP from

Table 1. APP modifications and the effects on localization and Aβ production

Modification:	Causes Localization to:	Cleavage Increased:	Amyloid Beta Production:
N-Glycosylation	PM	α-secretase	↓
O-Glycosylation	PM	α-secretase	↓
Phosphorylation			
Ser655	TGN	α-secretase	↓
Thr668	N/A	β-secretase	↑
Ubiquitination			
Lys651	PM	α-secretase	↓
Lys688	Golgi	α-secretase	↓
Palmitoylation	Lipid Rafts	β-secretase	↑

the membrane (Chun et al., 2015). Since α-secretase is found in the secretory pathway and at the plasma membrane, glycosylation of APP leads to decreased Aβ by colocalizing APP with α-secretase.

APP is can also be phosphorylated at ten sites; eight are located in the cytoplasmic domain, and the other two are found in the ectodomain (Gandy et al., 1988). The more influential phosphorylation sites occur in the cytoplasmic domain, and the most notable of the 8 are Ser655

and Thr668. Ser655 can be phosphorylated by protein kinase c (PKC), Ca^{++}/Calmodulin-dependent protein kinase II, or APP kinase I (Gandy et al., 1988; Isohara et al., 1999; Suzuki et al., 1992). The majority of phosphorylated Ser655 is found in mature APP, while phosphorylated Thr668 is found in immature APP, as this modification normally takes place in the ER (Oishi et al., 1997; Muresan & Muresan, 2012). Thr668 can be phosphorylated by glycogen synthase kinase 3β (GSK3β), cyclin dependent kinase 5 (CDK5), CDK1, stress-activated protein kinase 1β (SAPK1β), c-jun N-terminal protein kinase (JNK) (reviewed in Wang et al., 2017). Ser655 phosphorylation leads to increased APP trafficking to the TGN, and reduced trafficking to the lysosomes. This leads to decreased Aβ production by localizing more APP within the secretory pathway, therefore placing APP in an ideal location for α-secretase cleavage. However, with Thr668 phosphorylation, there is no effect on APP trafficking but an increase in Aβ production is seen do to modified protein interactions. Thr668 causes a conformational change which blocks the binding of Fe65 at the YENPTY motif (Ando et al., 2001). Fe65 is an adaptor protein that is known to cause translocation of APP to the plasma membrane when bound (Sabo et al., 1999). By blocking the binding of Fe65 through Thr668 phosphorylation, Aβ secretion is increased. One of the other notable sites for APP phosphorylation is Tyr687, which causes APP trafficking to the secretory pathway, increasing α-secretase cleavage and therefore Aβ production (Zambrano et al., 2001).

APP is also ubiquitinated within its cytoplasmic domain. Ubiquitination signals for degradation, translocation, and aids in protein-protein interactions. There are two main sites for this modification in APP, Lys651 and Lys688. Lys651 ubiquitination, in neurons, leads to increased APP trafficking to the plasma membrane, and increase α-secretase cleavage (Watanabe et al., 2012). Lys688 ubiquitylation aids in translocation of APP to the Golgi,

therefore decreasing Aβ production as well (Hiltunen et al., 2006). Overall, ubiquitination seems to be nonamyloidogenic.

Palmitoylation can occur on two cysteine residues in APP, specifically Cys186 and Cys187, but only around 10% of all APP undergoes this modification (Bhattacharyya et al., 2013). Palmitoylation is the process of adding fatty acids to cysteine residues and occurs in the ER. Once the palmitoylated APP reaches the plasma membrane, it is more likely to be sorted into lipid rafts, due to the added fatty acid. BACE-1 is highly localized to lipid rafts within the plasma membrane, so there is a higher probability for β cleavage of APP, increasing Aβ production following palmitoylation.

Regulation of APP processing also occurs through protein interactions at the YENPTY motif within the cytoplasmic domain, and through dimerization. While the mechanism is not clearly understood, X11 proteins play a role in regulation of APP processing. If X11 is overexpressed, the half-life of APP is significantly increased, and the production of sAPPα and Aβ is inhibited (Sastre et al., 1998). This indicates that binding of X11 to the YENPTY motif of APP results in inhibition of both α-secretase and BACE-1 cleavage.

Further linking APP to development, the disabled (*Dab*) gene family proteins interact with APP at the YENPTY motif and increase the concentration of mature cellular APP, although the mechanism by which this occurs is not well understood. These adaptor proteins regulate the positioning of neurons throughout the brain during embryogenesis. By increasing the amount of mature APP, there is more BACE-1 cleavage, due to the increased amount of substrate. Simply, mDab1 interaction with APP increases Aβ production. mDab1 can also bind to Fe65 to inhibit Fe65 interaction with APP to further increase Aβ production (Kwon et al., 2010).

Another regulation through protein interaction occurs with neuronal sorting protein-related receptor (SorLA). Inside of endosomes, SorLa allows for interaction between APP and retromer (Small et al., 2006). This signals for APP to go through retrograde transport to the TGN, before being cleaved by BACE-1 inside of the endosome. Interestingly, brain-derived neurotrophic factor (BDNF) upregulates SorLA expression via ERK signaling (Rohe et al., 2009). Overall, SorLA and APP interaction downregulates Aβ by initiating retrograde transport inside the endosome (Lee et al., 2008).

Dimerization of APP, whether homo- or hetero-, allows for cellular adhesion and communication, but also plays a major role in the regulation of APP processing. APP that is dimerized within the cytoplasmic domain is naturally done two ways; it can be via the GxxxG motif, or through GxxxA. GxxxG based APP dimers allow for BACE1 cleavage, and γ-secretase cleavage (Kienlen-Campard et al., 2002). However, if a point mutation occurs, and the motif switches to a GxxxA sequence, the ε cleavage from γ-secretase is allowed, to release the amyloid precursor protein intracellular domain (AICD), but the γ cleavage site is blocked (Kienlen-Campard et al., 2008). This means that the generally positive effects of the AICD are still allowed, but the production of Aβ is inhibited.

Neuronal activation regulates APP processing (Figure 3). When an action potential reaches the synaptic terminal of a neuron, there is an influx of calcium. This causes the fusion of synaptic vesicles with the plasma membrane so that the contained neurotransmitter may be released into the synaptic cleft. The fusion of synaptic vesicles leads to increased clatherin-mediated endocytosis so that the fused synaptic vesicles can be removed from the cellular membrane, however, with this upregulation of endocytosis, there is increased APP internalization (Cirrito et al., 2008). APP internalization leads to increased APP inside of early

and late endosomes where the majority of Aβ production occurs (Lah & Levey, 2000). In humans, brain areas with the most activity throughout life are the most prone to Aβ accumulation

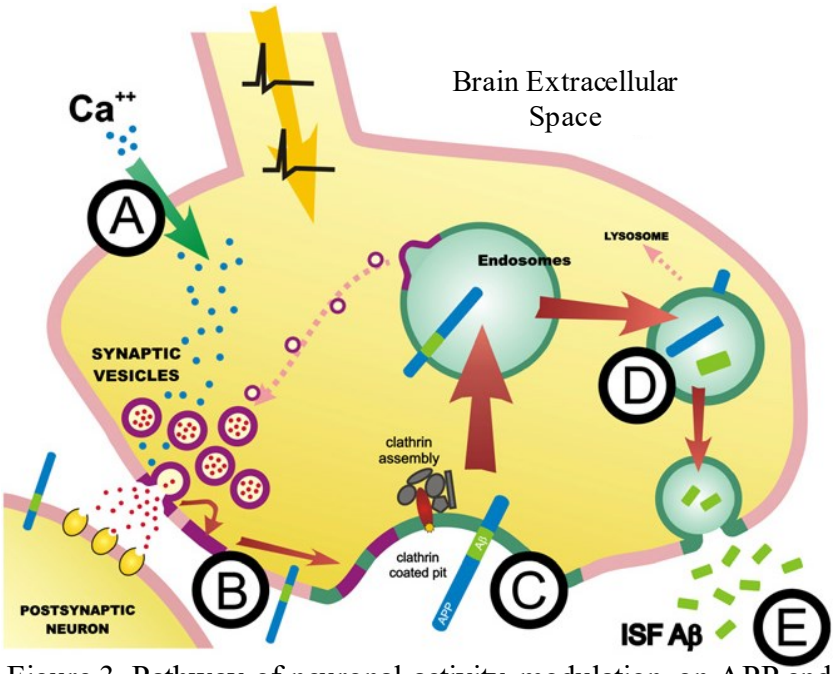

Figure 3. Pathway of neuronal activity modulation on APP endocytosis. (Adapted from Cirrito et al 2008).

(Buckner et al., 2005). Interestingly, there are also many links between stress-induced neuronal activity and AD (Wilson et al., 2005). Together, this indicates that neuronal activity leads to an increase in Aβ production by inducing colocalization of APP and BACE1. With this, there is a clear mechanism linking neuronal activity with increased Aβ production.

APP Processing. The majority of APP is processed by three families of enzymes; α-secretases, β-secretases and γ-secretases. APP is either cleaved by an α-secretase or β-secretase, but after cleavage by either of those enzymes, is always cleaved by γ-secretase (Figure 4).

α-secretase Cleavage. There are several zinc metalloproteinases that can function as α-secretases including, ADAM 9, ADAM 10, ADAM17 and ADAM19 (Allinson et al., 2003). ADAM10 is the most common α-secretase in neurons (Kuhn et al., 2010).

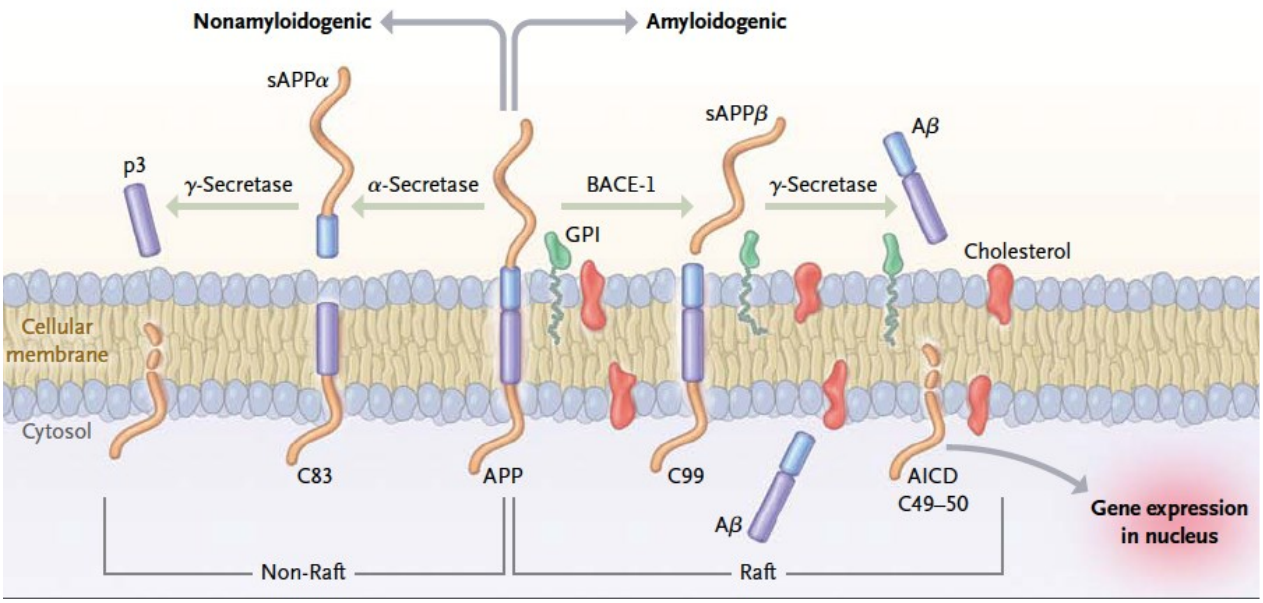

Figure 4. Summary of APP processing pathways
APP is either cleaved by α-secretase or BACE1 to enter the nonamyloidogenic or amyloidogenic, respectively. The nonamyloidogenic cleavage results in sAPPα and C83 (CTFα), whereas BACE1 cleavage results in sAPPβ and C99 (CTFβ). In either pathway, γ-secretase subsequently cleaves the membrane tethered CTF. In the nonamyloidogenic pathway, p3 is released. In the amyloidogenic pathway Aβ is secreted. In both pathways, the APP intracellular domain is liberated. (Adapted from Querfurth and LaFerla 2010).

Most α-secretase cleavage occurs at the plasma membrane (Sisodia, 1992), however, there is also α-secretase activity within the TGN where the majority of APP resides (Skovronsky et al., 2000). There are many ligands that are cleaved by α-secretases, including Notch, cadherins, IL-6 and tumor necrosis factor α, all of which are type I transmembrane proteins, like APP. When α-secretase cleavage occurs, the extracellular portion of the ligand is normally secreted.

Cleavage of APP by α-secretase is the first step in the non-amyloidogenic processing of APP. This processing of APP occurs between Lys16 and Leu17 within the E2 extracellular domain (Esch et al., 1990). This cleavage takes place within the Aβ sequence, therefore preventing the liberation of the Aβ peptide during subsequent cleavages. APP is cleaved by α-secretase at the plasma membrane or throughout the golgi apparatus and TGN. Cleavage the plasma membrane prevents APP from being endocytosed and deliver to early and late endosomes, where amyloidogenic cleavage would have likely occurred. Following α-secretase cleavage, secreted APP α (sAPPα) and the C-terminal fragment α (CTFα) are produced.

The sAPPα has been shown to be neurotrophic and neuroprotective by many studies (Hick et al., 2015; Plummer et al., 2016; Hefter & Braguhn, 2017). While the specific role of sAPPα, much like the role of APP is unclear, there have been many studies done that begin to elucidate possible mechanisms of action. In healthy patients, the cerebral spinal fluid (CSF) sAPPα levels are significantly higher than patients with AD (Lannfelt et al., 1995). That added with the fact that decreased sAPPα is correlated with decreased spatial memory in humans (Almkvist et al., 1997), is one of the primary arguments as to how sAPPα is neurotrophic.

Some argue that all of the neuroprotective functions of APP, like cell growth, cellular interactions and regulations, can be attributed solely to sAPPα (Hornsten et al., 2007). Furthering this, the deleterious effects in APP KO mice, like body and brain weight, decreased locomotion ability, and impaired LTP are fully restored with expression of sAPPα (Ring et al., 2007). While APP/APLP2 KO mice are not viable, the introduction of sAPPα rescues the lethal phenotype (Weyer et al., 2011). sAPPα has been seen to protect normal memory function and to increase neuronal survival (Meziane et al., 1998; Roch et al., 1994).

Extensive research has been done to evaluate sAPPα as a potential therapeutic target, not just for AD but for traumatic brain injuries as well. An induced expression of sAPPα resulted in decreased cell and axonal death and improved motor outcomes following traumatic injury in rats, compared to rats left to recover without intervention (Thornton et al., 2006). However, overexpression of sAPPα promotes tumorigenesis due to its role in cell growth (Chasseigneaux & Allinquant, 2012). For this reason, using sAPPα upregulation as a possible therapeutic target has many drawbacks (reviewed in Nhan et al., 2015).

Finally, there is evidence that the functions of sAPPα, and therefore the functions of APP come from the RERMS sequence, specifically the RER, within the E2 domain (Morrissey et al., 2019), at least when it comes to LTP. With infusion of the RERMS penta-peptide into rat brains, there is an increase in synaptic density as well (Roch et al., 1994).

Overall, the release of sAPPα, following α-secretase cleavage of APP, has neurotrophic and neuroprotective effects.

CTFα remains tethered to the membrane following α-secretase cleavage. CTFα is also known as C83 due to the number of amino acids left in the peptide. There is little known about any function CTFα might have other than remaining in the membrane until γ-secretase cleavage occurs to liberate the cytoplasmic domain of CTFα.

β-secretase Cleavage. β-site amyloid precursor protein cleaving enzyme 1 (BACE1) is a membrane bound aspartyl protease, indicating that it contains two aspartyl groups inside the active site, which resides in the extracellular space (Hong et al., 2000). Aspartyl groups are very acidic, which is what gives most membrane bound aspartyl proteases the ability to function at low pH's, between two and four. BACE-1 can be found in endosomes, the TGN, (Kinoshita et al., 2003) and within lipid rafts throughout the plasma membrane (Ehehalt et al., 2003). BACE-1

has optimal activity at low pH's, similar to that found in early and late endosomes. Similar to APP, BACE1 goes through many posttranslational modifications which effect its localization, and activity. BACE1 is synthesized in the endoplasmic reticulum, and immaturely, is a 501-amino-acid peptide (Capell et al., 2000). In the ER, BACE1 is glycosylated on four Asn residues (Haniu et al., 2000), and seven Arg residues (Costantini et al., 2007). Following these posttranslational modifications, BACE1 translocates to the Golgi apparatus where further glycosylation occurs as well as the removal of its prodomain by furin convertases (Bennett et al., 2000).

Mature BACE1 is trafficked to the plasma membrane. Phosphorylation on Ser498 of BACE1 signals for internalization from the membrane into endosomes (Pastorino et al., 2002). Palmitoylation of BACE1 also can occur on four Cys residues that are close to the transmembrane domain. (Vetrivel et al., 2009). The addition of fatty acids to those cysteine residues facilitate BACE1 translocation to lipid rafts within the plasma membrane.

BACE1 cleavage is the first step in the amyloidogenic processing pathway of APP. BACE1 cleaves APP within the E2 domain, much like α-secretase, but differs because its cleavage site, between amino acids 671 and 672 produces the N-terminus of the Aβ peptide (Figure 4). The beginning of Aβ is also the N-terminus of the CTFβ, which is slightly shorter than the CTFα. The cytoplasmic portion, sAPPβ, is shed following BACE1 action.

Not much is known about the function of sAPPβ; however, it is thought to hold many of the same neuroprotective properties as sAPPα, but it is 100x less powerful than sAPPα, so its effects are rarely seen (Furukawa et al., 1996). This proteolytic fragment does not regulate LTP

CTFβ remains tethered to the membrane following BACE1 cleavage. CTFβ is also known as C99 due to the number of amino acids left in the peptide. There is little known about

any specific unction CTFβ might have other than remaining in the membrane until γ-secretase cleavage occurs to liberate the cytoplasmic domain of CTFβ as well as Aβ.

γ-secretase Cleavage. The last proteolytic cleavage of APP is performed by γ-secretase, another aspartyl protease (Figure 4). Rather than being a single protein, γ-secretase is a complex containing four subunits with the catalytically active subunit being presenilin (PSEN) (reviewed in Steiner et al., 2008). PSEN has two homologs, PSEN1 and PSEN2, and either can be the catalytic subunit in unit in γ-secretase because they both contain two aspartyl groups inside of the sixth or seventh TMD (Wolfe et al., 1999). Both homologs contain nine TMD (Spasic et al., 2006), and to reach maturation, go through autocatalysis to become 2 subunits; the N-terminal fragment and the C-terminal fragment. Three other subunits are require for PSEN stability and optimal activity. Nicastrin (NCT), a type I integral membrane protein, is the second part of the γ-secretase complex (Yu et al., 2000), and may play a role in selecting substrates based on size (Shah et al., 2005; Dries et al., 2009). However, the role of NCT within the complex is still heavily debated. Anterior pharynx-defective phenotype (Aph-1) is another subunit in γ-secretase (Goutte et al., 2002), and while the exact function has not been elucidated there is speculation that Aph-1 might be a scaffold protein, required for interaction of NCT and PSEN1 or PSEN2 (LaVoie et al., 2003). The presenilin enhancer protein (Pen-2) completes the γ-secretase complex, contains two TMD (Francis et al., 2002), is thought to stabilize presenilin (Prokop et al., 2004).

While identifying the specific structure of the γ-secretase complex has proven difficult, it has been demonstrated that NCT and Aph-1 bind together inside of the endoplasmic reticulum (LaVoie et al., 2003). Pen-2 binds to either of the presenilin's, and then combine with the

NCT/Aph-1 complex (Fraering et al., 2004). These four subunits have been identified to be necessary and sufficient for γ-secretase cleavage.

Following initial cleavage of APP by α-secretase or BACE1, a CTF is left behind tethered to the plasma membrane, which is the substrate for γ-secretase. APP is processed by γ-secretase is a step-wise fashion within the TMD (Figure 4 and 5). There are three cleavages that are each performed around three amino acids apart (as reviewed in Haass et al., 2012). The first cleavage is after either amino acid residues 48 or 49 and is called ε-cleavage.

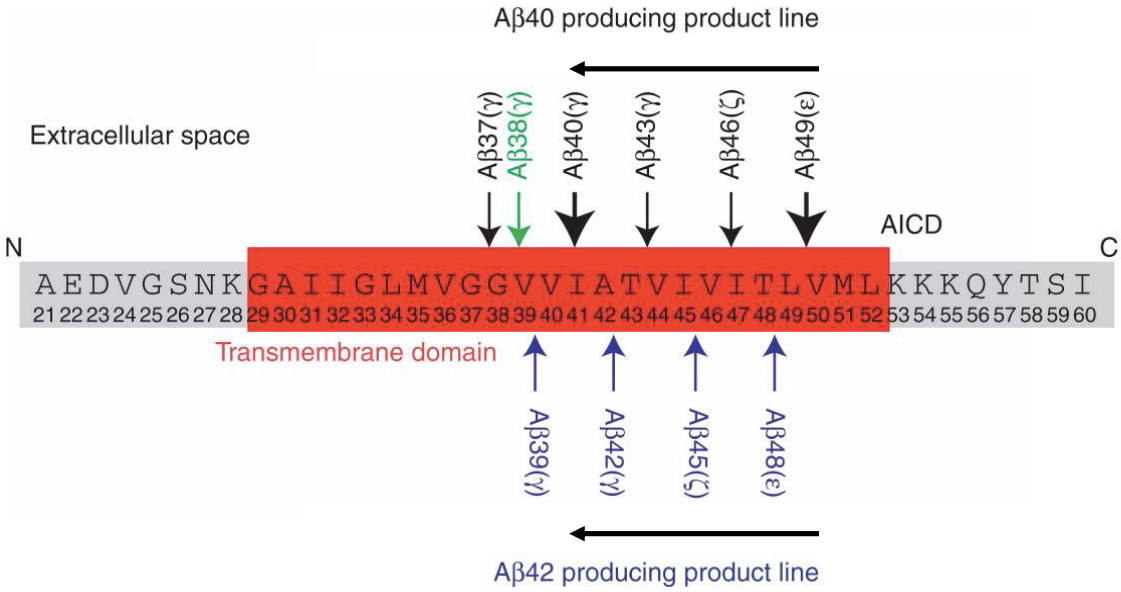

Figure 5. Sequential Cleavages of APP by γ-secretase
ε-cleavage occurs first, and is typically after either amino acid 48 or 49. ξ-cleavage is second, and happens following residues 46 or 45. γ-cleavage is last, and is variable, happening after residues 37, 38, 39, 40, 42, or 43. Here, the two main Aβ isoform production pathways are depicted. (Adapted from Haass et al 2012.)

Subsequently, ξ-cleavage takes place after residues 46 or 45. The last cleavage, called γ-cleavage, is the most variable. This cleavage can take place after amino acids 37-43, but normally takes place following residues 40 or 42 resulting in fragments named for their length, i.e. Aβ40 or Aβ42.

The fragments liberated by γ-secretase cleavage depend on the prior processing of APP. If α-secretase was responsible for initiating APP processing, then γ-secretase cleavage results in a p3 peptide (Haass et al., 1993b), which is secreted extracellularly, and seems to be of little pathologically importance. If BACE1 was responsible for beginning APP processing, then γ-secretase cleavage liberates the neurotoxic Aβ peptide (Seubert et al., 1992). γ-secretase also produces AICD following ε-cleavage of APP, regardless of prior cleavages (Gu et al., 2001).

Although the AICD is produced in both pathways of APP processing, there is evidence that the fragment is only transcriptionally active when rendered from the amyloidogenic pathway (Nalivaeva & Turner et al., 2013). Since the AICD is a short and unstable peptide, confirming its effects has been difficult. Within the AICD, the YENPTY motif and its possible interaction with Fe65 aids to keep the peptide stable for translocation to the nucleus. Inside of the nucleus, the AICD is thought to act as a transcriptional activator of many genes including, *GSK3β,* and *NEP (*Kim et al., 2003; Grimm et al., 2015). Increased levels of GSK3β protein could lead to an increased amount of APP phosphorylated at Thr668, which as aforementioned, leads to an upregulation in Aβ production by increasing BACE1.

Aβ Overview. AD is a very complex disease, and there are many mechanism's responsible for the pathology. The most widely accepted hypothesis used to describe AD is the amyloid cascade hypothesis. The amyloid cascade hypothesis suggests that AD occurs due to an imbalance between Aβ production and clearance.

The Aβ peptide is the hallmark of AD. There are many isoforms of Aβ, which are dependent on the γ-cleavage of γ-secretase. The most neurotoxic isoforms are $A\beta_{40}$ and $A\beta_{42}$ (Chen et al., 2017). After secretion, Aβ peptides can aggregate together to form oligomers, which recently, have been noted to be the most pathological (Selkoe & Hardy, 2016). Aβ

oligomers can aggregate to create fibrils, which can further aggregate to become senile plaques. Aβ treated hippocampal neurons have LTP inhibition and reduced synaptic spine density (Shankar et al., 2008). Interestingly, Aβ secretion following upregulated neuron activity negative feedbacks to depress synaptic activity (Kamenetz et al., 2003). Levels of soluble Aβ early in life correlate to the levels of toxic multimers seen with aging (Fisher et al., 2016).

Aβ Clearance. Decreased clearance of Aβ is also noted as a possible reason for amyloid deposition and plaque formation. Aβ is cleared from the brain both enzymatically, and non-enzymatically. Enzymes involved in proteolytic degradation of Aβ include neprilysin (NEP) (Iwata et al., 2001), insulin-degrading enzyme IDE (Hersh, 2006), and metalloproteases (MMPs), specifically MMP2, MMP9 and MMP14 (Yan et al., 2006; Liao & Van Nostrand, 2010).

NEP is a zinc-metalloprotease that regulates Aβ levels through proteolytic cleavage. Both $A\beta_{40}$ and $A\beta_{42}$ levels were 2-fold higher in NEP knockout mice compared to wild type controls (Iwata et al., 2001) indicating NEPs role as an Aβ mediator. NEP degradation of Aβ likely occurs in presynaptic terminals because of its classification as a type II membrane-associated peptidase (Turner et al., 2001; Iwata et al., 2004). There is evidence to suggest that NEP accounts for 50% of total Aβ clearance (Saito et al., 2003). While NEP is known to clear monomeric Aβ, whether it clears toxic oligomers is controversial. There is evidence demonstrating NEP clearing Aβ oligomers (Huang et al., 2006; Kanemitsu et al., 2003), but there are also contradictory findings (Meilandt et al., 2009; Lessring et al., 2003).

IDE is also a zinc-metalloprotease, but unlike NEP is known to only degrade monomeric Aβ due to its unique structure (Shen et al., 2006). IDE resembles a clam shell, with the internal pocket being the active site for Aβ degradation. Due to the small nature of the opening to the

internal pocket of IDE, oligomers cannot fit and therefore, are not degraded by IDE. IDE is known to be localized in the cytosol (Falkevall et al., 2006) and the mitochondria (Leissring et al., 2004), but other cellular locations are less certain including endosomes, the endoplasmic reticulum and lysosomes.

While MMP2, 9 and 14 have been implicated in Aβ clearance, compared to NEP and IDE, MMPs are very weak modulators of Aβ levels. Deletion of either MMP2 or MMP9 resulted in small, but significantly different, changes in Aβ throughout the cortex and hippocampus (Yin et al., 2006). However, it seems that with increases in Aβ deposition, production of MMPs is upregulated (Yin et al., 2006).

Non-enzymatic pathways include bulk flow into the CSF by ISF draining through the perivascular basement membranes (Bedussi et al., 2015), and transfer across the blood-brain barrier (BBB) by LRP1 (Storck et al., 2015). While Aβ can freely flow through the glial barrier of the BBB, the endothelial tight junctions prevent free transfer of Aβ into the peripheral circulation (Storck et al., 2015). In order to transport Aβ through these tight junctions specialized transporters like low-density lipoprotein receptor-related protein 1 (LRP1). Various studies suggest that LRP1 is the main transporter of Aβ across the BBB (Ito et al., 2006). LRP1 transports $A\beta_{40}$ much fasters than $A\beta_{42}$ (Storck et al., 2015; Deane et al., 2008).

Factors Affecting AD Pathology

Physical Activity. There are many different types of exercise, ranging from aerobic exercise, like running, to strength training, like lifting weights. There are also forms of multicomponent training that involved aerobic, muscle strength and coordination exercises. All forms of exercise provide important health benefits such as increases in cardiac output, which

leads to increased blood flow. In the brain, raised blow flow can provoke numerous neurotrophic mechanisms, like angiogenesis, synaptogenesis and neurotransmitter uptake (Zigmond et al. 2012; Radak et al. 2014). Exercise seems to be neuroprotective against neurodegenerative diseases, such as AD, by attenuating their progression (reviewed in Sutoo & Akiyama 2003; Leem et al 2011; Zigmond et al 2012). In addition to the different types of exercise, there are divisions of physical activity that define whether an activity is exercise.

Divisions of Physical Activity. Physical activity involves any voluntary movement of the body, that expends energy. Physical activity includes, but is not limited to, running a marathon, biking, swimming, and even gardening. There is acute physical activity and chronic physical activity (Figure 6). Chronic physical activity refers to repetitive bouts of physical activity, whereas acute physical activity refers to a single session. Acute physical activity can be divided into normal daily physical activity and exercise. Normal daily physical activity includes things like gardening, walking to a class, and cooking dinner. Exercise is more structured than normal daily physical activity and includes swimming, playing in a pick-up basketball game or going for

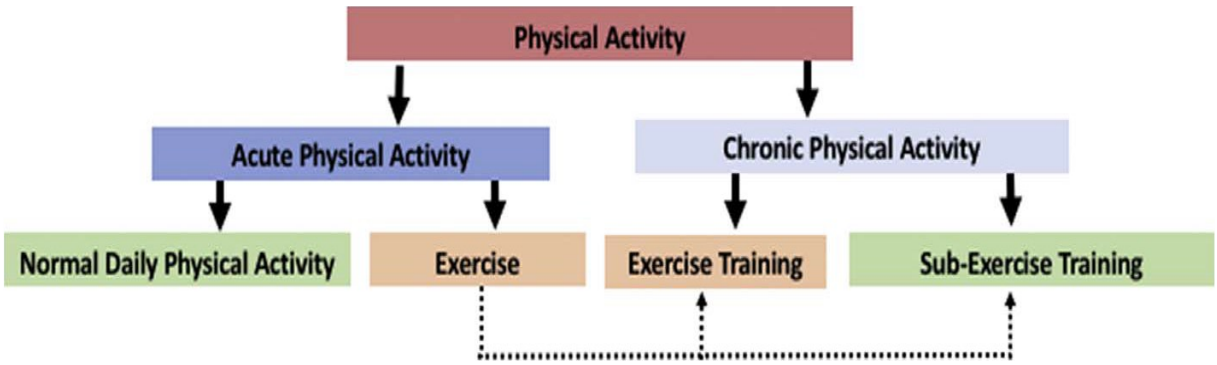

Figure 6. Divisions of physical activity. (Adapted from Yuede et al., 2018).

a walk after dinner. Chronic activity is typically structured and is a regimen that repeats with a long-term goal of improving overall health.

Chronic physical activity can be split into exercise training and sub-exercise training.

Exercise training (ET) is chronic physical activity, where a measurable training effect occurs. The training effect could be a variety of things including increased muscle strength, or increased levels of a Krebs cycle enzyme. Citrate synthase is a commonly used to confirm exercise training (Moore et al., 2016; Thomas et al., 2020). Once the exercise bouts are no longer creating a measurable training effect, it becomes sub-exercise training. For example, if someone ran 2 miles a day for 4 weeks, and each time they ran it, they were improving their times, and it was easier, that is exercise training, but once running 2 miles becomes easy and is not improving general fitness, it is sub-exercise training.

Exercise Training and AD. There are many health benefits of ET including a decreased risk for AD development (Laurin et al., 2001; Wilson et al., 2002). Many exercise studies are performed using transgenic mouse lines. There are two forms of exercise administered in the literature, forced and voluntary. Forced increases the psychological stress associated with the exercise, but additional variables such as exercise intensity or length can be controlled. Forced running is administered by placing mice on treadmills, while voluntary running typically takes place on a wheel. Forced running decreased Aβ compared to sedentary animals (Yuede et al., 2018), suggesting that if the intensity of the exercise is high enough, the negative effects of psychological stress from being forced to run, are overcome by the benefits of ET. There seems to be an intensity "threshold" where exercise above the threshold show beneficial effects, but exercise below shows no neuroprotective effects (Yuede et al., 2018). The beneficial properties of exercise in relation to AD, such as decreased Aβ and increases in the proteins responsible for Aβ clearance are increased in a dose-dependent manner (Moore et al., 2016; Thomas et al., 2020). Therefore, high intensity exercise is more beneficial than moderate intensity exercise in

the attenuation of AD progression. In a transgenic mouse model, such as APP/PS1, an exercise regimen of 15 m/min, 60 min/day, 5 days a week that lasts for 8 weeks is above the intensity threshold and will elicit an exercise training effect (Yuede et al., 2018).

Exercise training causes an increase in brain-derived neurotrophic factor (BDNF) (Huang et al., 2014; Ferris et al., 2007). BDNF is a marker for general brain health due to its neuroprotective properties (Acheson et al., 1995). High levels of *BDNF* expression are seen in the hippocampus and cortex, as well as other areas crucial for memory development. BDNF contributes to synaptic growth and plasticity and modulates long-term potentiation in the hippocampus (Lu et al., 2014). In people with AD, lower levels of BDNF are observed (reviewed in Ng et al., 2019). Increased levels of BDNF due to exercise could be one of many ways ET leads to cognitive benefits as seem in many humans afflicted with AD, as well as mouse models (Chapman et al., 2013; Yu et al., 2006; Thomas et al., 2020).

Stress. Stress can be anything that causes a temporary upset in homeostasis. Stress can be categorized as physical or psychological. In general, stress can be regarded as a mental or physiological challenge. Physical stress could include having an illness, going for a walk, or being outside in the cold. Psychological stress is emotional or cognitive stress. Examples include feeling guilty after an argument with a friend, losing a loved one, or being worried about an upcoming exam. While acute stress in generally harmless, prolonged stress increases the risk for development of AD, and can exacerbate symptoms (Dong & Csernansky, 2009; Wilson et al., 2003, 2006; Machado et al., 2014).

Molecular Pathway of Stress. When a stressor is detected the hypothalamic-pituitary-adrenal (HPA) axis and sympathetic nervous system are activated. The periventricular nucleus is in the hypothalamus and responds to neuronal impulses indicating stress by activating

specialized neurons to secrete corticotropin-releasing factor (CRF). CRF travels to the anterior pituitary gland and stimulates the production and secretion of adrenocorticotropic hormone (ACTH). Once ACTH reaches the adrenal cortex, it signals for the production and secretion of glucocorticoids (GC), including cortisol (Ulrich-Lai & Herman, 2009). Generally, cortisol is responsible for increasing blood glucose levels during a stressful event and modifying fat and protein metabolism (Stephens & Wand, 2012). However, when in high concentrations, cortisol can also influence learning and memory and cardiovascular function (Adinoff et al., 2010). While the neuroendocrine response to all stressors is largely the same, physical stress is typically accompanied by an upregulation in growth hormone levels, unlike psychological stress (Ranabir & Reetu, 2011).

Stress and AD. While the mechanism whereby stress increases the progression of AD is not completely known, there are several studies that demonstrate that chronic stress affects AD through increased GC signaling following prolonged HPA axis activation (Salvagioni et al., 2017; Rehman, 2002). Cortisol levels correlate with the severity of cognitive decline seen in AD (Pedersen et al., 2001), illustrating that amplified GC levels may have a role in overall cognition deficits seen in those with AD. In transgenic AD mouse models, mice treated with a corticosteroid had increased APP, Aβ, and BACE levels (Green et al., 2006). This demonstrates a direct link between increased GC levels are AD progression through Aβ production. Recently, one study revealed a link between GC-related pCREB transcriptional activation and increased BACE1 (Choi et al., 2017). These studies have depicted a relationship between stress signaling and increased Aβ production, leading to exacerbation of AD symptoms, therefore decreasing cognition. There is also evidence that increased CRF signaling through the CRF receptor 1 (CRFR1) is present in AD patients (Behan et al., 1995), and can increase AD pathogenesis

(Campbell et al., 2015). CRFR1 signaling influences Aβ production by modulating α-, β-, and γ secretases (Park et al., 2015; Thathiah & Destrooper, 2011). Interestingly, temporary activation of CRFR1 pathways decreases Aβ production by shifting APP processing towards the α-secretase-mediated pathway; however, with chronic activation of CRFR1, APP processing shifts towards the β-secretase-mediated pathway, resulting in toxic Aβ peptides (Willem et al., 2015).

Stress and Exercise. Although exercise is a considered a physiological stressor, chronic exercise may be protective against stress (Tsatsoulis & Fountoulakis, 2006). Chronic psychological stress and chronic exercise stress differ at a molecular level. When evaluating the effects of both types of chronic stressors, those who participated in the chronic exercise regimen had the same levels of cortisol as sedentary "non-stressed" individuals when awakening (Labsy et al., 2013). However, subjects who underwent chronic psychological stress had increased cortisol levels upon awakening compared to controls (Wüst et al., 2000). Interestingly, the conversion of cortisol to cortisone increases directly with the amount of exercise completed but does not increase proportionally to chronic psychological stress (Gourané et al., 2005). Therefore, the difference in chronic psychological or physical stress may be related to the conversion of cortisol into cortisone.

Another way in which physical and psychological stress differ is through the modulation of an endocannabinoid, anandamide (AEA), which easily crosses the blood-brain barrier and seems to play a role in improving mood following exercise. AEA increases following exercise (Heyman et al., 2012) but decreases following psychological stress (Gunduz-Cinar et al., 2013). Interestingly, psychological stress increases fatty acid amide hydrolase, which breaks down AEA (Reich et al., 2009). As mentioned earlier, exercise leads to an increase in plasma BDNF,

however, there is evidence to suggest that AEA is required for BNDF levels to remain elevated after exercise (Heyman et al., 2012), and it may serve as a mediator of the BNDF effect on long-term potentiation and memory. As an endocannabinoid, AEA binds to cannabinoid receptor type 1 (CB1R) and exercise leads to an increase in the density of CB1R in the hippocampus in rats; a region of high importance for memory formation (Hill et al., 2010). If CB1Rs are blocked, exercise-induced BDNF increase is diminished (Ferreira-Vieira et al., 2014), illustrating a relationship between BDNF levels and AEA binding. The exact mechanism of this relationship is unknown.

Voluntary exercise is generally more beneficial than forced exercise of the same intensity because it is perceived as less of a psychological stressor (Yuede et al., 2009 & Yuede et al., 2018). However, at higher intensities forced exercise still slows the progression of AD pathology (Yuede et al., 2018). Chronic exercise can train the body to be more resilient to both psychological and physical stressors, which can prevent exacerbation of AD (Cavalcante et al., 2017).

Serotonin. Serotonin has been linked to many behaviors and processes, including food intake, motor function, neuron firing rate, sexual arousal, reproduction abilities, mood and fetus maturation. Recently, serotonin has been shown to decrease the production of amyloid beta, when SSRI's are used, further linking A.D. and depression.

Serotonin (5-HT) is a tryptophan derivative, that is produced following two subsequent enzymatic modifications by tryptophan hydroxylase and l-amino acid decarboxylase (Azmitia, 2010). Tryptophan is an essential amino acid and therefore is acquired by dietary intake only; however, it is not found in high quantities in the body due to the competition for transport into the brain with other, more abundant amino acids, and due to the average diet (Azmitia, 2010).

Tryptophan is more concentrated in fruits, vegetables and nuts, rather than meat, because photosynthesis is coupled to tryptophan production (Azmitia, 2010). As a consequence of the minuscule tryptophan availability, serotonin synthesis is limited to mast cells and neurons, and is produced in small quantities as well (Azmitia, 2010).

Despite the limited abundance of serotonin, it still plays a major role in many human processes. This can be attributed to the diversity of receptors (5-HT_R) and the presence of binding proteins that aid to transport of 5-HT to specific regions. There are 7 main 5-HT_R families ($5HT_1R$- $5HT_7R$) (Bockaert et al., 2010).

Serotonin and AD. Serotonin concentrations effect the progression of AD. When selective serotonin reuptake inhibitors (SSRIs) are used, in mice and humans, a reduction in Aβ levels is seen in both the hippocampus and the cortex (Fisher et al., 2016). Upon binding of serotonin to certain receptors, specifically G protein-coupled receptors that activate cyclic AMP dependent kinase (PKA), lead to Raf activation. Then, Raf activates MEK, which phosphorylates ERK. Phosphorylated ERK can either remain in the cytoplasm where it acts to phosphorylate proteins, or it is transported to the nucleus to act as a transcription factor. In the case of Aβ level reduction, it appears that ERK phosphorylates α-secretase, increasing its activity (Fisher et al., 2016). However, there were no reductions in BACE-1 activity. This indicates that the increased activity of α-secretase limits the amount of available ligand for β-secretase to cleave. The stimulation of serotonin receptors effects the production of Aβ rather than the clearance. Serotonin receptor subtypes 4, 6, and 7 regulate Aβ concentrations (Fisher et al., 2016). Interestingly, even though inhibiting any one receptor does not alter Aβ levels, stimulation of one is enough to reduce Aβ levels by the same amount as when all of them are stimulated. This suggests redundancy in this mechanism.

Serotonin and Exercise. Exercise may elevate serotonin levels by increasing the likelihood that tryptophan crosses the BBB (Patrick & Ames, 2015). Since exercise requires muscle activity, and active muscles require branched-chain amino acids, this limits the competition of BBB transport for tryptophan. Exercise increases serotonin in the cortex (Meeusen & De Meirleir, 1995), but decreases 5HT levels throughout the hippocampus immediately following exercise (Dey et al., 1992).

There are clear links between AD and exercise training, as well as AD and stress, and AD and serotonin however, to date, there have been no studies examining the effects of the interaction of exercise training and isolation stress on the serotonergic system in an AD model. This study aims to identify the effect of an exercise training regimen and isolation stress on serotonin levels in the cortex and the hippocampus, as well as serotonin receptors 4, 6 and 7. Other aims of this study is to investigate a possible correlation in serotonin and Aβ levels following treatment, in addition to exploring a relationship of BDNF and CRF levels with serotonin levels.

MATERIALS AND METHODS

Experimental Design

Forty-eight APP/PS1 mice with the appswe/ps1de9 trans genes and a C57BL/6J genetic background were divided into 8 different groups in this study. All procedures involving the live mice were approved by Missouri State IACUC under protocol 2019-1 (Appendix). Four female and four male groups were further separated by the type of housing they were subjected to, as well as by the exercise treatment they received (Figure 7).

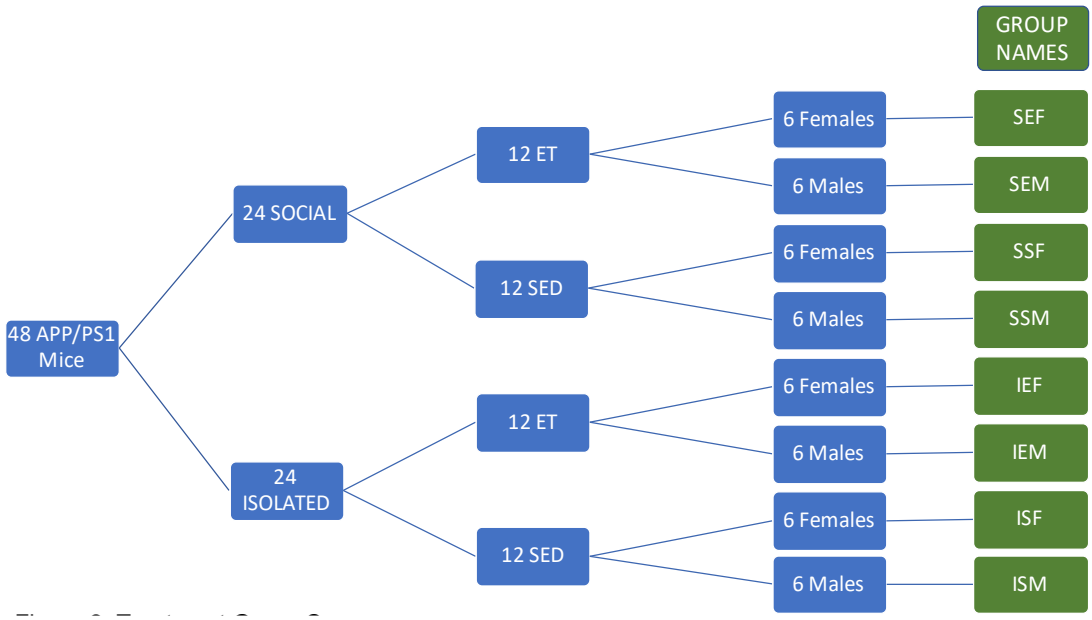

Figure 7. Experimental design for animal groups.

Animal Treatment. All mice were obtained through an in-house breeding colony. In order to determine which pups had the APP/PS1 genes, genotyping was preformed between 12 and 21 days of age (Figure 8).

Genotyping. Briefly, tail samples were taken from each mouse, a number assigned, and the tail marked for identification. QIAamp DNA Mini Kit from QIAGEN was used to extract DNA, and the samples were then analyzed by PCR using 3 primers from IDT based off of the Tg(APPswe,PSEN1dE9)85Dbo-Chr9 genotyping protocol from JAX laboratories, as well as GoTaq Green Master Mix from Promega. One of the primers is found in both the wild type and the transgenic mice, acting as the reverse primer, while each of the other two primers are specific to either the APP/PS1 or wildtype genotype. In hemizygous mice, which was the genotype utilized, both of the genotype specific primers work. PCR products were run on a 2% agarose gel using 1X TAE. For sample visualization, ethidium bromide was used. A 100-bp ladder was ran as a scale to predict the band sizes. The expected band sizes were142 bp for a transgenic mouse,

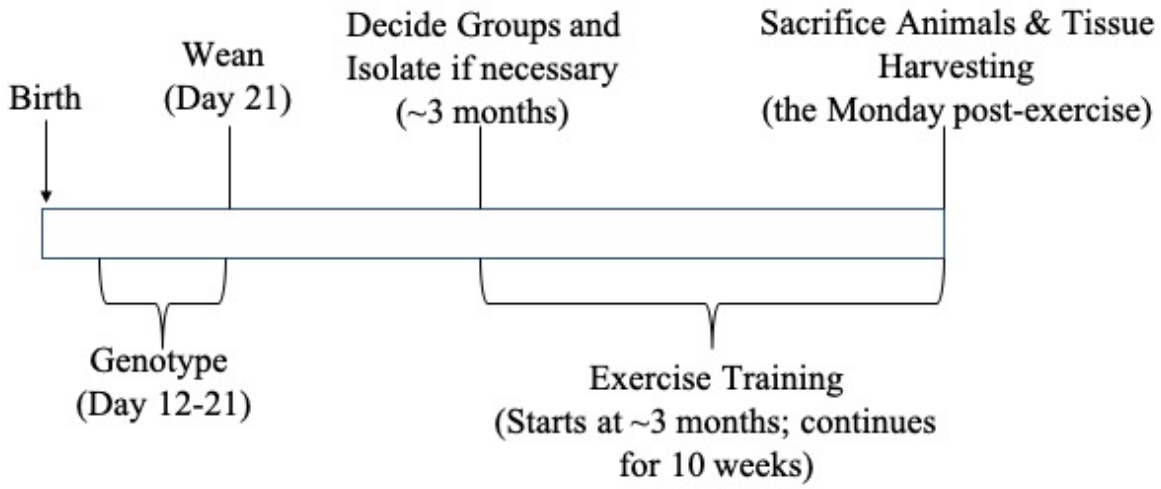

Figure 8. Experimental timeline.

and 265 bp for a wild type. Hemizygous mice had both bands. Mice used in studies were tattooed for identification.

Animal Housing. Routine care of the animals was handled by the animal husbandry staff at Missouri State University. Mice were kept on a 12-hour light/dark cycle, and receive food and water *ad libitum.* All mice will be socially housed until three months of age (Figure 3). The socially housed animals were kept in ventilated cages with three to four mice per cage. At three months, the mice in the IEF, IEM, ISF, or ISM group were moved to isolated housing (Figure 3). These animals lived alone in the same cages, but a divider reduced the cage to about a third of its normal area. Cages for isolated housing were placed so that the mice could not see other mice.

Exercise Training Regimen. Exercise training (ET) began concurrently with housing relocation (Figure 3). All ET sessions occurred during the dark cycle and took place in a darkened room. All mice were placed on a 6-lane treadmill equipped with a mild electric current at the end of the lane for encouragement. Gentle mechanical encouragement was also provided by the researchers, who were present for all ET sessions to records levels encouragement needed for each animal. Mice were kept on the same lane for the duration of the training. The first week of ET was an acclimation period, where the mice ran at increasing speeds until they reached 20 meters per minute. After the acclimation week, the ET mice ran at 20 meters per minute for 60 minutes Monday through Friday for 10 weeks. The sedentary mice were placed on the treadmill, with the same conditions as the exercised mice, but did not run.

Tissue Collection and Preparation

Dissections. The mice were dissected on the Monday following completion of the 10-week exercise training regimen.

Preparations and Anesthesia. First, each mouse was weighed and the mass was recorded. Simultaneously, the isoflurane vaporizer was prepped for use. Each mouse was placed into the

anesthesia chamber. When breathing became slowed and the mouse became lethargic, the mouse was placed onto dissection tray where a tube continuously supplied the mouse with isoflurane as anesthesia. After checking to ensure the mouse is void of reflexes, the feet were pinned down.

Profusion. An incision was made at the xyphoid process, and the cut continued superiorly. The ribs were cut through and the region was blunt dissected, exposing the heart. The right atrium was cut while a saline syringe punctured through the left ventricle. The heart was profused with a minimum of three 2.5 ml syringes of saline and continued until the heart stopped bleeding. Once completed, the heart was removed to ensure lifelessness of the animal.

Brain Extraction. Dissecting forceps were clasped onto the skull, an incision was made at the base of the head, and the region was blunt dissected. While ensuring the scissors were always pointed up, so that the brain was not punctured, a cut was made, through the skull, towards the frontal bone. To expose the brain, the sides of the forceps were used to ply back the skull on either side of the cut. The brain was then carefully removed from the skull and placed onto a petri dish on top ice. The carcass was moved to the solei extraction station.

Brain Dissection. First, the brain was separated into hemispheres. The medial brain surface was placed facing upwards, with the cerebellum facing to the left. The brainstem was teased out by rolling it into the rest of the brain and then down, exposing the hippocampus. Using the pointed side of a metal spatula, the hippocampus was lifted out revealing white matter. The cusp of the cortex that was over the hippocampus was then sliced off, and the white matter was removed to the greatest extent possible. This is repeated for both hemispheres. The hippocampi and cortices were weighed and flash frozen in liquid nitrogen before being stored at -80°C. Dissections of WashU mice separated the brain into multiple regions to store for potential future projects. However, this is the method used for all mice relevant to this project.

Solei Extraction. The carcass was placed in prone position and the skin of the inferior hind leg was removed. One side of the forceps was slid between the tibia and the lower hind leg muscles, and then the calcaneal tendon was cut. The muscles were then flipped back to reveal the underside. The bright red thin muscle was located and identified as the soleus. One side of the forceps was slid under the soleus to separate it from the mass of muscles, and the superior tendon was cut. The soleus was removed and weighed before being flash frozen and then stored at -80°C. This was repeated for both hind legs.

Tissue Preparation. For sequential extraction of proteins from brain tissues to be used in ELISAs three buffers were used: PBS, Triton, and Guanidine. To make the PBS buffer, 9.9 ml of 1x PBS was combined 100 ul of a protease inhibitor, made using apotinin and leupeptin. The triton buffer was made by combining 100 ul of Triton X-100, 9.9 ml of PBS and 100 ul of a protease inhibitor which was previously made at Washington University. The guanidine buffer was made by mixing 9.9 ml of 5M Guanidine-Tris buffer and 100 ul of a protease inhibitor. All buffers were placed on wet ice to chill prior to using.

Each sample tube first received 10 ul of the PBS buffer per 1 mg of tissue weight. The tissues were then homogenized using a pestle by turning 12 turns to the right, 12 to the left and then 12 right turns again. The pestle was cleaned with 70% ethanol and MiliQ water between each sample. The samples were centrifuged for 25 minutes at max speed at 4°C. The supernatant was collected into another tube and kept on ice. This was repeated with triton instead of PBS, using the pellet remaining following supernatant removal. After spinning again, the triton fraction was collected into another tube and chilled on ice. Guanidine was added to the residual tube, at the same volume as the other two buffers. Samples were sonicated for 18 pulses at 50% amplitude. The sonicator tip was cleaned with MiliQ water and dried between each sample to

prevent contamination. The tubes were spun at max speed for 25 minutes at 4°C, and the supernatant was collected.

Protein Analysis

Total Protein Assay. Samples were first diluted, using MiliQ water, to a concentration of 1:50. For each well a sample was plated on, 100 ul of diluted sample was needed. Separate curves had to be made for each extraction buffer used to account for excess background due to the buffer interactions. For each curve 2143.75 ul of MiliQ water was combined with 43.75 ul of the given extraction buffer (PBS/Triton/Guanidine). Eight tubes were used to make each curve. The first tube received 250 ul of the H_20/buffer mixture. For the second tube, 62.5 ul of the Bovine Serum Albumin (BSA) from the ThermoFischer Pierce Protein Assay BCA and 437.5 ul of the H_20/buffer mixture were combined and vortexed. The final concentrations of all of the tubes were as followed: Tube 1- 0 μg/ml, Tube 2- 2500 μg/ml, Tube 3- 125 μg/ml, Tube 4- 62.5 μg/ml, Tube 5- 31.25 μg/ml, Tube 6- 15.625 μg/ml, Tube 7- 7.81 μg/ml, and Tube 8- 3.9μg/ml.

A 96-well plate was loaded with 100 ul per well of sample or curve in duplicates. Simultaneously, the working reagent from the ThermoFischer Pierce Protein Assay BCA kit was prepared: 50 parts of reagent A, 48 parts of reagent B, and 2 parts of reagent C were mixed (1 part = 40 ul). The plate was loaded with 100 ul per well of the working reagent and incubated at 37°C while covered until a color developed. Plates were read using a plate reader at 562 nm. The concentrations given were exported to Microsoft excel, where they were multiplied by 50 and divided by 1000 to reach mg/ml and account for the prior dilutions.

ELISA Analysis of Amyloid Beta. Beginning on the first day, a 6 ml solution of carbonate coating buffer and 20 ug/ml of the HJ2 antibody (for $A\beta_{40}$) or 10 ug/ml of the HJ7.4

antibody (for $A\beta_{42}$) was prepared and mixed by inversion 4 to 5 times. Using a 96-well plate, 50 ul of the solution was placed into each well. The plate was sealed and labeled, and then left to incubate overnight in the 4°C refrigerator on the rotator.

The following day, 2% BSA-PBS was prepared; some was diluted to 1% and the rest was stored for up to 3 days. The plate was removed from the rotator and washed using the automated plate washer, after making sure the washer had been primed using 1xPBS-0.05% Tween 20. Residual liquid remaining following plate washing was removed, and 190ul of 1% BSA-PBS was placed into each well. Then the plate was incubated for an hour at 37°C. While plate was incubating, samples and curve were prepared. Sample buffer (SB) was made by combining 5 ml of 3M Tris, 250 ul of 10% Azide, 12.5 ml of 2% BSA-PBS, 500 ul of 100x Protease Inhibitor, and 31.75 ml of 1xPBS-0.05% Tween 20. Samples were diluted using SB to different concentrations based on what buffer was used to extract the solute from the brain tissue: PBS: 1:10, Triton: 1:20, Guanidine: 1:5,000. The SB used to make standard curves was spiked with the corresponding buffer at different concentration equivalent to the sample concentrations: PBS: 5.94 ml of SB and 600 ul of PBS, Triton: 5.7 ml of SB and 300 ul 1% of Triton-PBS buffer, and Guanidine: 5.999 ml of SB and 1 ul of 5M Guanidine-Tris buffer.

The curve was set up using 10 tubes. The stock tubes of Aβ were centrifuged briefly prior to pipetting from so to ensure even distribution of the dissolved protein. In the first tube, a solution 680 ul formic acid (FA) and 8 ul Aβ were combined and vortexed to ensure even distribution of Aβ. In the second tube, 8 ul of the previous tube, 80 ul of 3M Tris, and 712 ul of SB were combine and vortexed. For the third tube, 12 ul of the previous tube and 988 ul SB were combined, and mixed by pipetting. For the remaining tubes, excluding the last tube, 300 ul of the previous tube and 600 ul of SB were combined and mixed by pipetting. The last tube received

600 ul of SB. The calculated standard concentrations were as follows: B: 0 pg/ml, S1: 1200 pg/ml, S2: 400 pg/ml, S3: 133.3 pg/ml, S4: 44.4 pg/ml, S5: 14.8 pg/ml, S6: 4.9 pg/ml, and S7: 1.6 pg/ml.

The plate was loaded with the samples and the curves in duplicate or triplicate. After the 60-minute incubation was complete the plate was washed again with 1xPBS-0.05% Tween 20, but the residual 1xPBS-0.05% Tween 20 was left in the wells. Wells were vacuumed dry, and immediately filled with 50 ul of each sample. Samples were mixed by pipetting prior to loading wells. The loaded plate was sealed and labeled and place into the 4°C refrigerator on the rotator overnight.

For day three, some 2% BSA-PBS was diluted to 6 ml of 0.05% BSA-PBS-T20 using 1xPBS-0.05% Tween 20. This was combined with the HJ5.1 Biotin antibody at a concentration of 1:250. The plate was removed from the refrigerator and washed with 1xPBS-0.05% Tween 20 using the plate washer. The residual fluid was removed, and then the plate was loaded with 50 ul per well of the HJ5.1 antibody in the 0.05% BSA-PBS-T20 mixture. The plate was incubated at 37°C for 90 minutes, while 6 ml of 0.5% BSA-PBS-T20 was made using the stored 2% BSA-PBS and 1xPBS-0.05% Tween 20. The 0.5% BSA-PBS-T20 was combined with the strep-Poly HRP40 antibody at a concentration of 1:500. Upon completion of the incubation, the plate was washed with 1xPBS-0.05% Tween 20 and the residual liquid was removed. The plate was loaded with 50 ul per well of the strep-Poly HRP40 mixture, and then covered and placed on the shaker at room temperature for 90 minutes. Afterwards, the plate was washed with 1xPBS-0.05% Tween 20 and the leftover liquid was removed. The plate was loaded with 50 ul per well of sigma superslow 3,3′,5,5′-Tetramethylbenzidine Liquid Substrate (TMB).

Following TMB addition, plates were read at 2, 6 and 10 minutes using a plate reader. The raw concentrations were exported to Microsoft excel where they were multiplied by 50 and then divided by 1000 to get the concentration prior to dilutions. In order to normalize data, substrate concentrations were divided by total protein concentrations. Concentrations reported here are normalized proteins and expressed as picograms of amyloid per mg/ml of total protein. Averages were found as well as standard deviations where applicable.

Citrate Synthase Analysis. Citrate synthase activity was tested using a kit and protocol from Sigma Aldrich (cat No. Cs0720). Both solei muscles from each mouse were weighed, placed together and 2 ml of CelLytic MT Cell Lysis Reagent (Sigma Aldrich No. C3228) was added for each gram of tissue. Samples were homogenized and centrifuged at 20,000 x *g* for 10 minutes. The supernatant was collected and stored at -4°C.

A master mix was made containing 186 ul of 1x assay buffer, 2 ul 30 mM Acetyl CoA, and 2 ul 5,5′-Dithiobis-(2-nitrobenzoic acid) (DNTB) for each sample. After aliquoting the master mix into each well, 8 ul of sample was added. Samples were loaded in triplicate. Absorbances were read at 412 nm on a BioTek Epoch plate reader for 1.5 minutes each time. Following collection of baseline absorbances, 10 ul of oxaloacetate was added to each well. Final absorbances were read.

To calculate enzyme activity, the change in baseline absorbance was subtracted from the change in final absorbance. The calculated absorbance was multiplied by 0.2 ml, and 20 to account for the reaction volume and the dilution factor respectively. Then, the value was divided by 13.6, 0.552 cm, .002 ml to account for the extinction coefficient of the TNB (the visual product produced from DNTB reaction), the pathlength of absorbance of the 96 well plate, and the volume of the enzyme in the sample respectively. To obtain the citrate synthase activity per

gram of tissue, the previously calculated value was divided by the weight of the solei muscles. The triplicate groups were averaged together.

RESULTS

Standard Curve Practice

Single Practice Curve. To start practicing ELISA techniques, a single curve was produced and loaded 10 times. The plate layout is depicted in Figure 9.

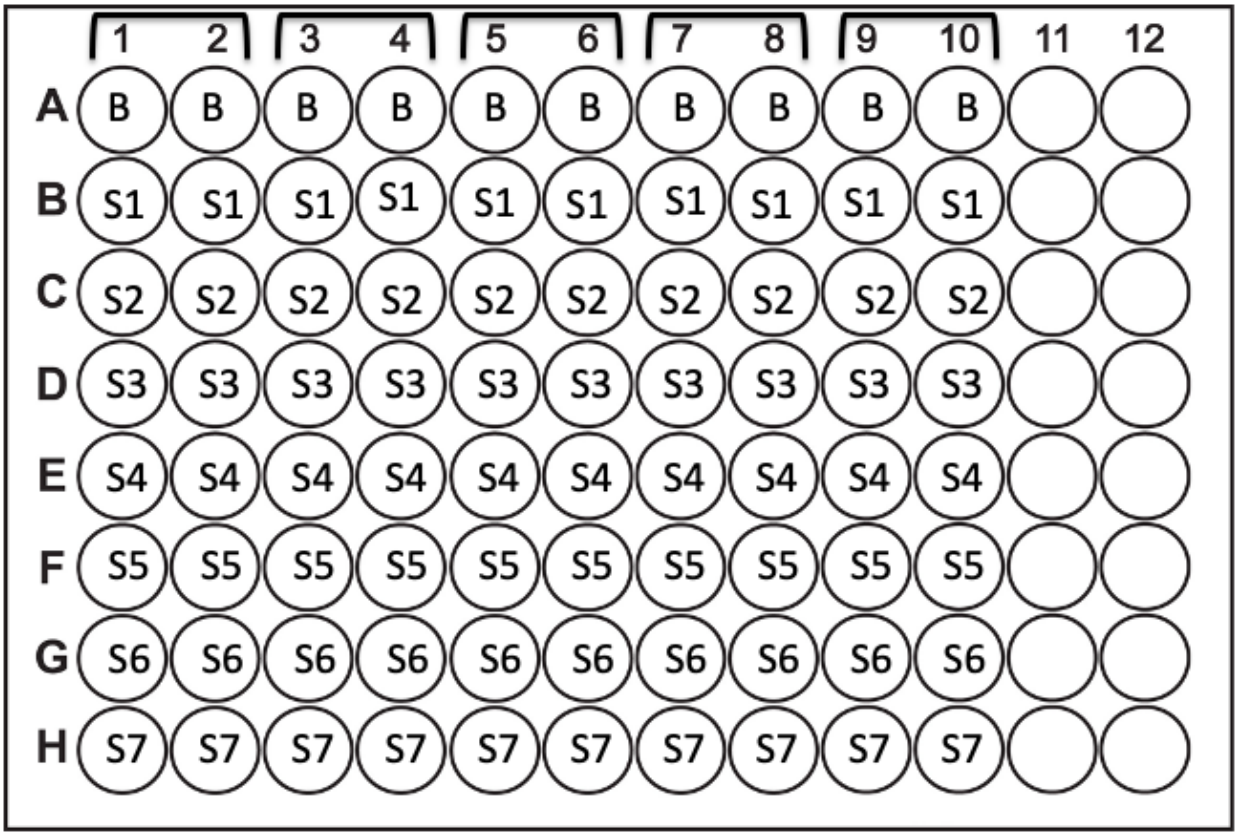

Figure 9: Loading Pattern of Single $A\beta_{40}$ Standard Curve in 5 Duplicate pairs
Loading pattern of 96-well plate used for $A\beta_{40}$ curve. "S" means standard, and "B" represents blank. The number represents where in the curve the standard falls, with 1 being the beginning of the dilution, and 7 being the final product. The standard concentrations were as follows: B: 0 pg/ml, S1: 1200 pg/ml, S2: 400 pg/ml, S3: 133.3 pg/ml, S4: 44.4 pg/ml, S5: 14.8 pg/ml, S6: 4.9 pg/ml, and S7: 1.6 pg/ml. One curve was loaded in duplicate 5 times. Duplicate pairs are indicated by black brackets around lane numbers.

The plate was loaded in duplicate; meaning that A1 was loaded, then A2, and then B1 and B2, all the way down through H2. Then, columns 3 and 4 were loaded and so on.

Sample concentrations are shown in Table 2. Blanks were all zeroed out, and although not shown, absorbance values were between .06 and .07. Standard 1, which contains the largest concentration, had to be covered across all 5 duplicate pairs as it was over the top of the curve. This allows for accurate concentrations of actual samples to be given. Between standard 2 and standard 7 values typically decrease with the exception of standards 5 or 6 (Figure 10). Within standards, there is some variance (Table 3). For duplicate pairs 3, 4, and 5, standard 7 is less than zero, like the blank. When comparing the average of each standard to the calculated values of that standard the standard deviation is fairly low with the exception of Standard 1 (Table 3). Standard 1's average concentration is quite a bit lower than the calculated value. For this curve, there is more variation between samples within the same standard, than between the average and the calculated concentration. The R^2 value of the experimental concentrations was 0.7843 (Figure 10).

Table 2: Concentrations of Single $A\beta_{40}$ Standard Curve in 5 Duplicate pairs

Sample ID	Concentrations (pg/ml)									
	Duplicate pair 1		Duplicate Pair 2		Duplicate pair 3		Duplicate pair 4		Duplicate Pair 5	
Blank	<0.00	<0.00	<0.00	<0.00	<0.00	<0.00	<0.00	<0.00	<0.00	<0.00
Standard 1	Masked[1]	Masked[1]	Masked[1]	Masked[1]	Masked[1]	Masked[1]	Masked[1]	Masked[1]	Masked[1]	Masked[1]
Standard 2	Out[2]	254.48	Out[2]	Out[2]	Out[2]	363.18	367.49	Out[2]	296.13	392.27
Standard 3	185.23	136.48	152.87	143.81	127.16	131.48	125.89	115.26	111.55	131.85
Standard 4	63.48	41.61	51.46	44.91	39.04	42.32	36.80	39.88	37.83	41.22
Standard 5	19.05	5.10	8.59	2.06	0.98	1.00	0.73	5.04	<0.00	<0.00
Standard 6	31.44	14.76	21.70	17.96	12.07	11.92	11.44	3.63	7.69	11.50
Standard 7	7.98	3.52	2.68	22.53	<0.00	<0.00	<0.00	<0.00	<0.00	<0.00

[1] After reading, points were covered to improve R^2 value and make other readings more accurate.
[2] Values were over the top of the curve and unable to be calculated.

Triple Practice Curves I. To continue practicing ELISA techniques, three curves were made and loaded in triplicate. This means that columns 1 through 3 were loaded together,

then 4-6 and then 7-9.

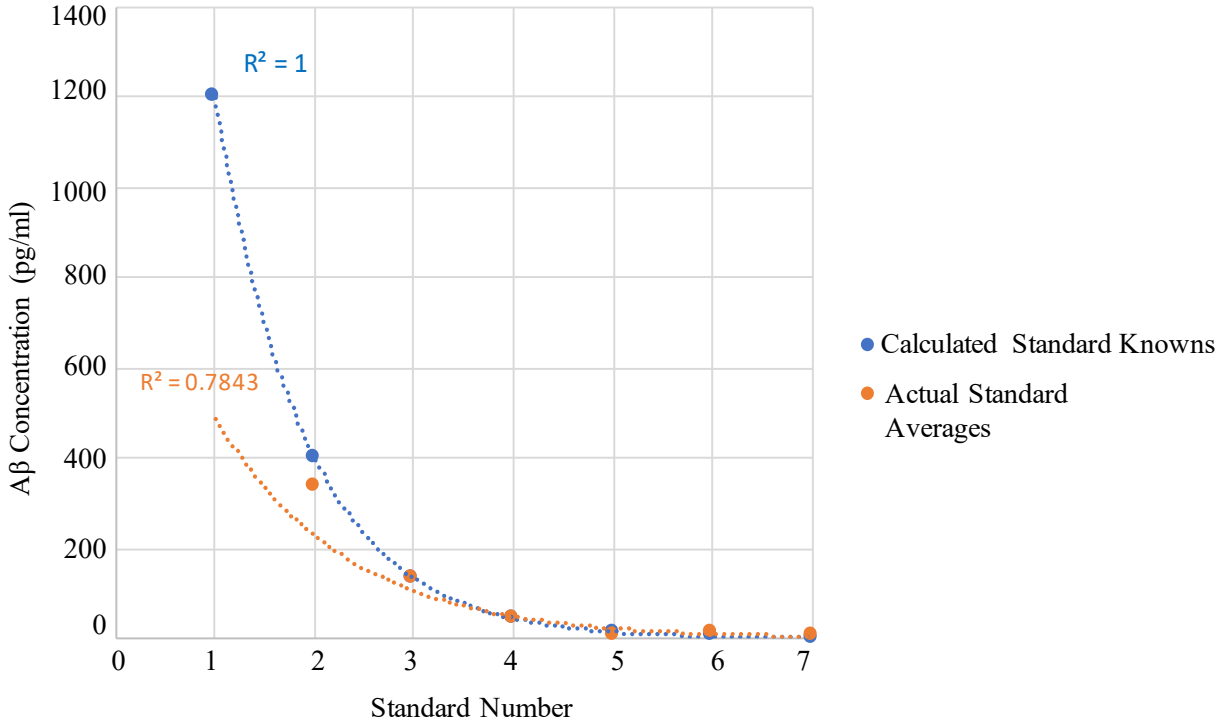

Figure 10: Comparison of Experimental and Calculated Amyloid Standard Concentrations for the Single $A\beta_{40}$ Standard Curve
Calculated concentrations of the standard curve were compared to the actual values. Calculated values are shown in blue with a R^2 of 1, while the experimental values are shown in orange with a R^2 of .7843. The calculated standard concentrations were as follows: B: 0 pg/ml, S1: 1200 pg/ml, S2: 400 pg/ml, S3: 133.3 pg/ml, S4: 44.4 pg/ml, S5: 14.8 pg/ml, S6: 4.9 pg/ml, and S7: 1.6 pg/ml.

The plate layout is depicted in Figure 11. Curve concentrations are shown in Table 4. No curves had decreasing tends moving from standard 1 to 7 (Table 4-5 and Figure 12).

All of the standards for curve 2, except for standard 1, had a concentration at or below the background, resulting in a "LOW" reading (Table 4-5). This was also the case for curve 1 standards 6 and 7, as well as curve 3 standards 5-7 (Table 4-5). Standard deviation within standards increased compared to the last practice curves (Table 3 and 5). Overall, concentrations throughout the plates are extremely low, increasing variance between the expected values and the

experimental values (Table 5). R^2 values were unobtainable due to the lack of an overall decreasing trend within the curves (Figure 12).

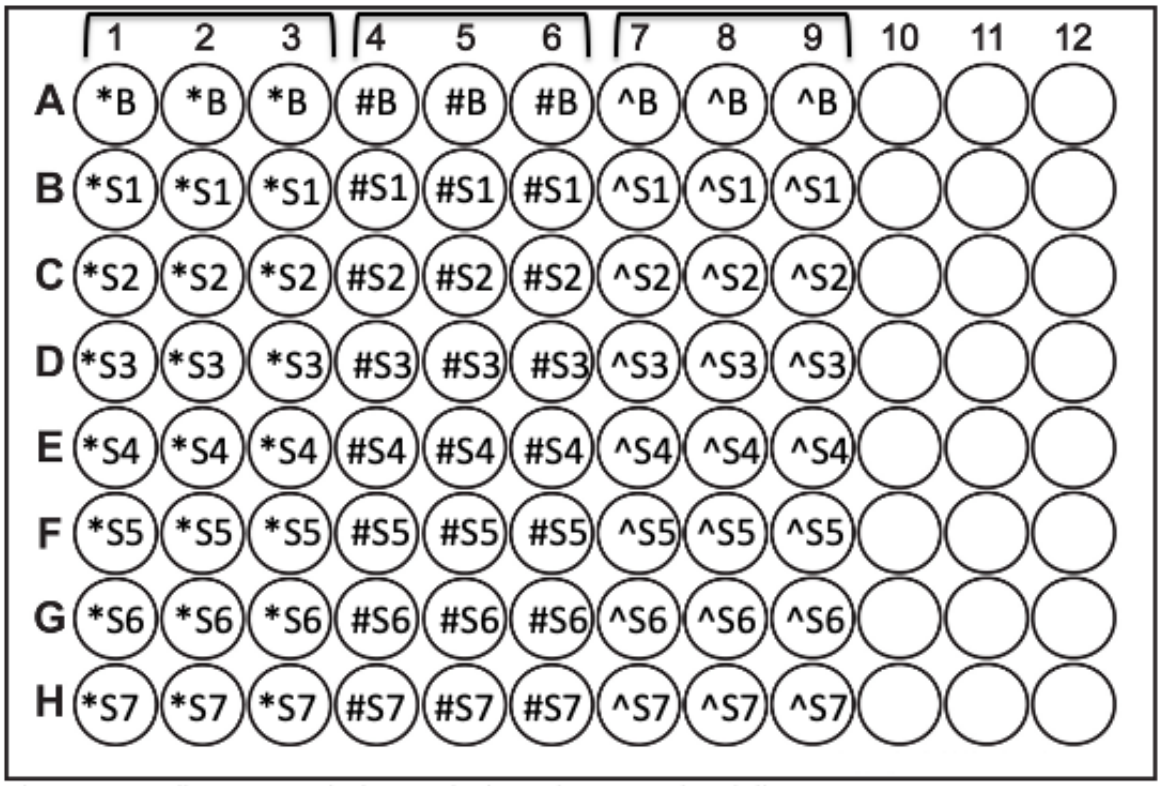

Figure 11: Loading Pattern of $A\beta_{40}$ Standard Practice Curves in Triplicate #1
Loading pattern of 96-well plate used for $A\beta_{40}$ curve. "S" means standard, and "B" represents blank. The number represents where in the curve the standard falls, with 1 being the beginning of the dilution, and 7 being the final product. The standard concentrations were as follows: B: 0 pg/ml, S1: 1200 pg/ml, S2: 400 pg/ml, S3: 133.3 pg/ml, S4: 44.4 pg/ml, S5: 14.8 pg/ml, S6: 4.9 pg/ml, and S7: 1.6 pg/ml. Three curves were loaded in triplicate. The first curve is indicated with a *. The second curve is indicated with a # and the third curve is indicated by a ^. Triplicate groups are indicated by black brackets around lane numbers.

Triple Practice Curves II. To continue practicing ELISA techniques, three more curves were made and loaded in triplicate. The loading pattern of the plate is depicted in Figure 13. The curve concentrations are shown in Table 6. The blank fell between <0.00 pg/ml and 9.301 pg/ml across all points of each curve. Standard 1 across all three curves was masked as it was over the top of the curve. Standard 2 was also above the curve in one point for curve 1 and 2 points for

Table 4: Concentrations of $A\beta_{40}$ Standard Practice Curves in Triplicate #1

Sample ID	Concentrations (pg/ml)								
	Curve 1 (*)			Curve 2 (#)			Curve 3 (^)		
Blank	<0.00	<0.00	<0.00	<0.00	<0.00	<0.00	<0.00	<0.00	<0.00
Standard 1	274.91	276.35	252.10	11.62	<0.00	8.18	262.21	211.84	250.90
Standard 2	259.58	289.59	279.646	LOW	LOW	LOW	275.23	217.44	295.08
Standard 3	271.32	286.09	180.72	LOW	LOW	LOW	293.32	262.71	304.75
Standard 4	351.32	234.61	246.42	LOW	LOW	LOW	290.54	231.52	303.45
Standard 5	117.37	86.95	94.79	LOW	LOW	LOW	LOW	LOW	LOW
Standard 6	LOW	LOW	LOW	LOW	LOW	LOW	LOW	LOW	LOW
Standard 7	LOW	LOW	LOW	LOW	LOW	LOW	LOW	LOW	LOW

curve 2 (Table 6). The blank values were close to standards 6 and 7. Curve 1 decreased moving from standard 2 to 7, with the exception of standard 7 (Table 7).

Curve 2 decreased moving down the curve (Table 7, and Figure 14). Curve 3 had decreasing concentrations moving down the curve with the exception of standard 7 (Table 7). Within the same standard, variance is slim in comparison to past curves (Table 3, 5, and 7). As is variance between the experimental and calculated values. For the experimental curve values the R^2 value were 0.88, 0.97 and 0.89 respectively (Figure 14).

WT/APP Practice Mice

After practicing ELISA techniques using only curves, practice samples were assayed. Practice cerebellum sections were provided by Dr. John Cirrito's lab at Washington University. Tissues were weighed, had proteins extracted from the brain, and then put through the ELISA procedure. Sixteen cerebellum sections were provided and weighed. Masses shown in Table 8. All masses were similar and fell within 19.0 g to 42.0 g. Weights did not play a role in amyloid

Table 5: Analysis of $A\beta_{40}$ Standard Practice Curves in Triplicate #1

Standard Number	Standard Deviation within Samples	Average Concentration (pg/ml)	Standard Deviation between Calculated and Average Values
Curve 1			
1	13.60	267.79	659.17437
2	15.29	276.27	87.49
3	57.05	246.04	79.70
4	64.25	277.45	164.76
5	15.79	99.70	60.03
6	N/A*	N/A*	N/A*
7	N/A*	N/A*	N/A*
Curve 2			
1	2.43	9.90	841.52778
2	N/A*	N/A*	N/A*
3	N/A*	N/A*	N/A*
4	N/A*	N/A*	N/A*
5	N/A*	N/A*	N/A*
6	N/A*	N/A*	N/A*
7	N/A*	N/A*	N/A*
Curve 3			
1	26.43	241.65	677.66
2	40.34	262.58	111.97
3	21.74	286.93	108.61
4	38.35	275.17	163.15
5	N/A*	N/A*	N/A*
6	N/A*	N/A*	N/A*
7	N/A*	N/A*	N/A*

* No data for this standard was available.

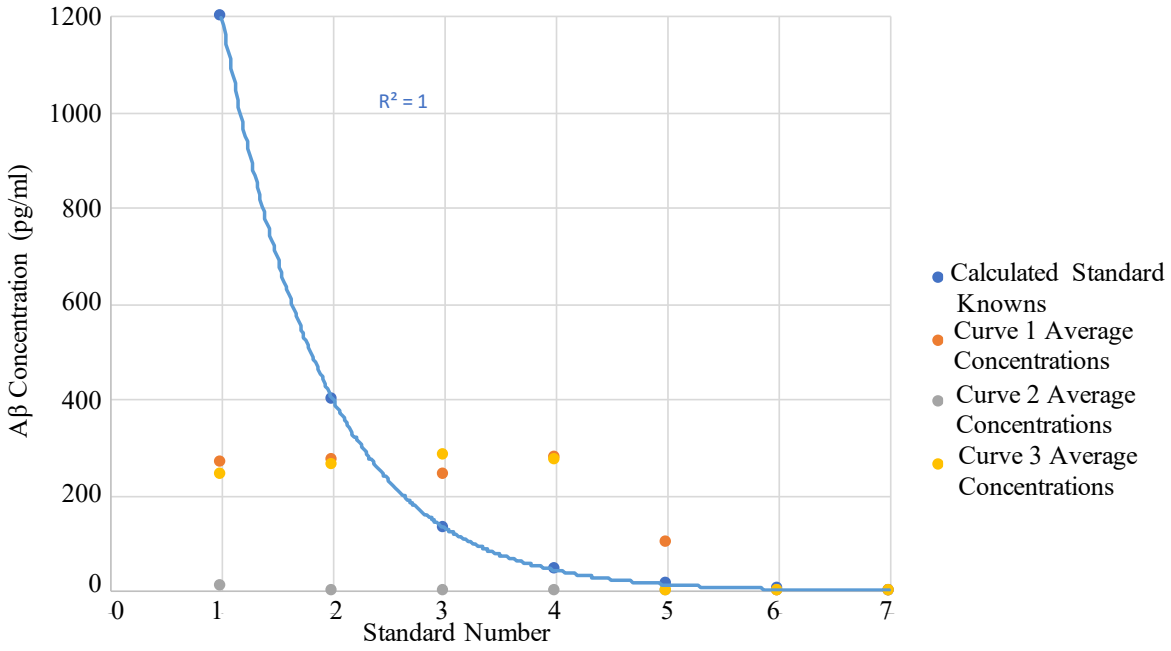

Figure 12: Comparison of Experimental and Calculated Amyloid Standard Concentrations of $A\beta_{40}$ Standard Practice Curves in Triplicate #1

Calculated concentrations of the standard curve were compared to the actual values. Calculated values are shown in blue with a R^2 of 1, while the experimental values are shown in orange for curve 1, grey for curve 2 and yellow for curve 3. R^2 were unable to be calculated as the values were too far off to generate a exponential equation. The calculated standard concentrations were as follows: B: 0 pg/ml, S1: 1200 pg/ml, S2: 400 pg/ml, S3: 133.3 pg/ml, S4: 44.4 pg/ml, S5: 14.8 pg/ml, S6: 4.9 pg/ml, and S7: 1.6 pg/ml.

concentrations as they were normalized for. Following sequential extraction using PBS, triton and guanidine buffers, a total protein assay, BCA, was ran for each buffer. The BCA plate layout for all three of the plates is depicted in Figure 15.

Total protein concentrations are listed in Table 9. The range for PBS concentrations was from 1.4 mg/ml to 5.1 mg/ml, but without the 5.1 mg/ml concentration the range became 1.4 mg/ml to 3.9 mg/ml. The range for triton concentrations was from 2.1 mg/ml to 3.8 mg/ml, and the range for guanidine concentrations was from 1.3 mg/ml to 3.7 mg/ml. However, if the 3.7 mg/ml data point is excluded, the range condensed to 1.3 mg/ml to 2.8 mg/ml. Between the three different buffers, looking at the same sample, seem to match up; that is, the samples with values

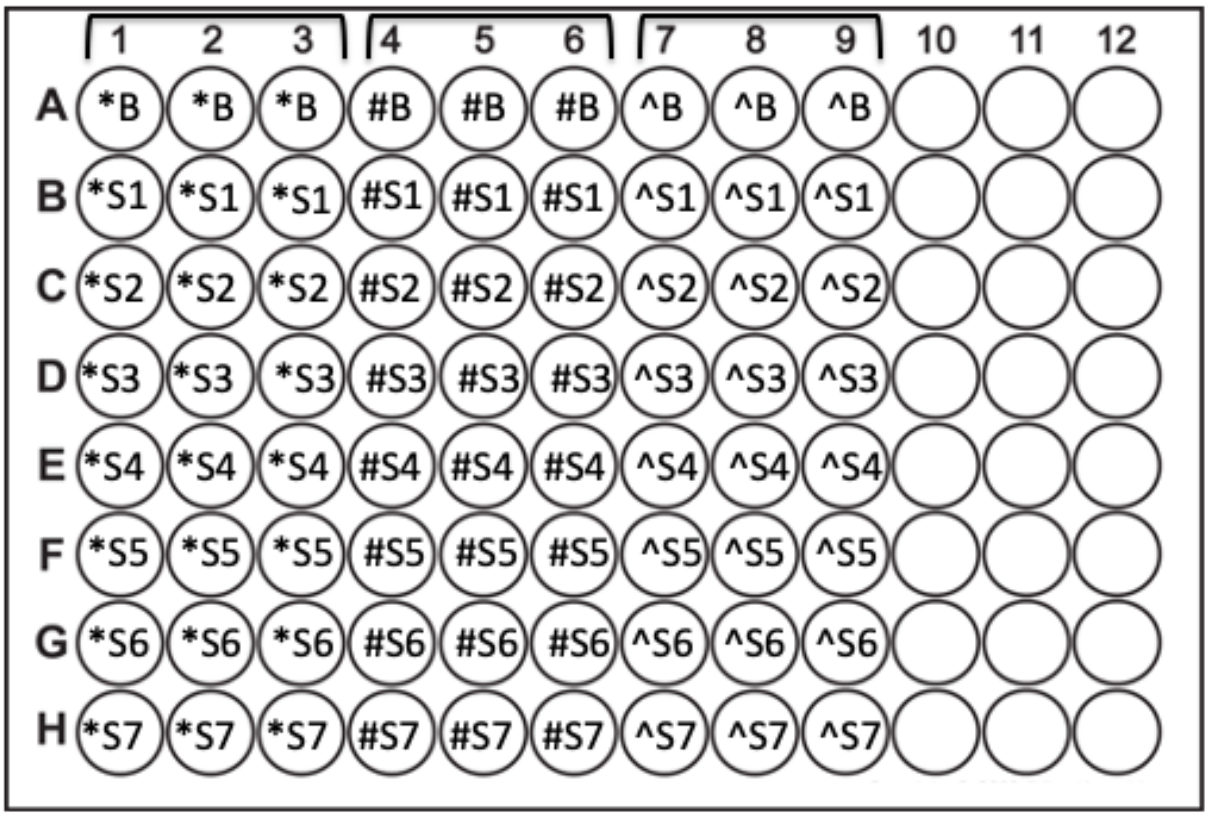

Figure 13: Loading Pattern of $A\beta_{40}$ Standard Practice Curves in Triplicate #2
Loading pattern of 96-well plate used for $A\beta_{40}$ curve. "S" means standard, and "B" represents blank. The number represents where in the curve the standard falls, with 1 being the beginning of the dilution, and 7 being the final product. The standard concentrations were as follows: B: 0 pg/ml, S1: 1200 pg/ml, S2: 400 pg/ml, S3: 133.3 pg/ml, S4: 44.4 pg/ml, S5: 14.8 pg/ml, S6: 4.9 pg/ml, and S7: 1.6 pg/ml. Three curves were loaded in triplicate. The first curve is indicated with a *. The second curve is indicated with a # and the third curve is indicated by a ^. Triplicate groups are indicated by black brackets around lane numbers.

Table 6: Concentrations of $A\beta_{40}$ Standard Practice Curves in Triplicate #2

Sample ID	Concentrations (pg/ml)								
	Curve 1 (*)			Curve 2 (#)			Curve 3 (^)		
Blank	6.356	5.001	2.535	2.388	3.882	5.276	4.822	9.301	<0.000
Standard 1	Masked	Masked	Masked	Masked	Masked	Masked	Masked	Masked	Masked
Standard 2	Out	380.281	381.076	OUT	401.721	OUT	339.102	293.319	316.951
Standard 3	137.821	145.828	132.435	161.83	153.431	151.567	102.975	118.408	105.668
Standard 4	37.693	36.183	35.787	41.302	38.729	36.603	25.161	25.327	25.382
Standard 5	10.722	8.843	8.832	8.907	8.363	34.904	6.123	6.568	6.685
Standard 6	10.294	5.89	3.745	4.252	3.577	3.303	2.766	3.661	4.536
Standard 7	10.241	7.917	8.598	3.904	2.609	3.45	5.033	4.304	6.165

Table 7: Analysis of $A\beta_{40}$ Standard Practice Curves in Triplicate #2

Standard Number	Standard Deviation within Samples	Average Concentration (pg/ml)	Standard Deviation between Calculated and Average Values
Curve 1			
1	N/A*	N/A*	N/A*
2	0.56	380.68	13.66
3	6.74	138.69	3.79
4	1.01	36.55	5.58
5	1.09	9.47	3.78
6	3.34	6.64	1.21
7	1.19	8.92	5.14
Curve 2			
1	N/A*	N/A*	N/A*
2	N/A*	401.72	1.22
3	5.47	155.61	15.75
4	2.35	38.88	3.94
5	15.17	17.39	1.82
6	0.49	3.71	0.87
7	0.66	3.32	1.18
Curve 3			
1	N/A*	N/A*	1200
2	22.90	316.46	400
3	8.24	109.02	133.3
4	0.12	25.29	44.4
5	0.30	6.46	14.8
6	0.89	3.65	4.9
7	0.94	5.17	1.6

* No data for this standard was available.

on the higher end of the PBS range tend to have higher values when compared to the ranges for the other two buffers as well.

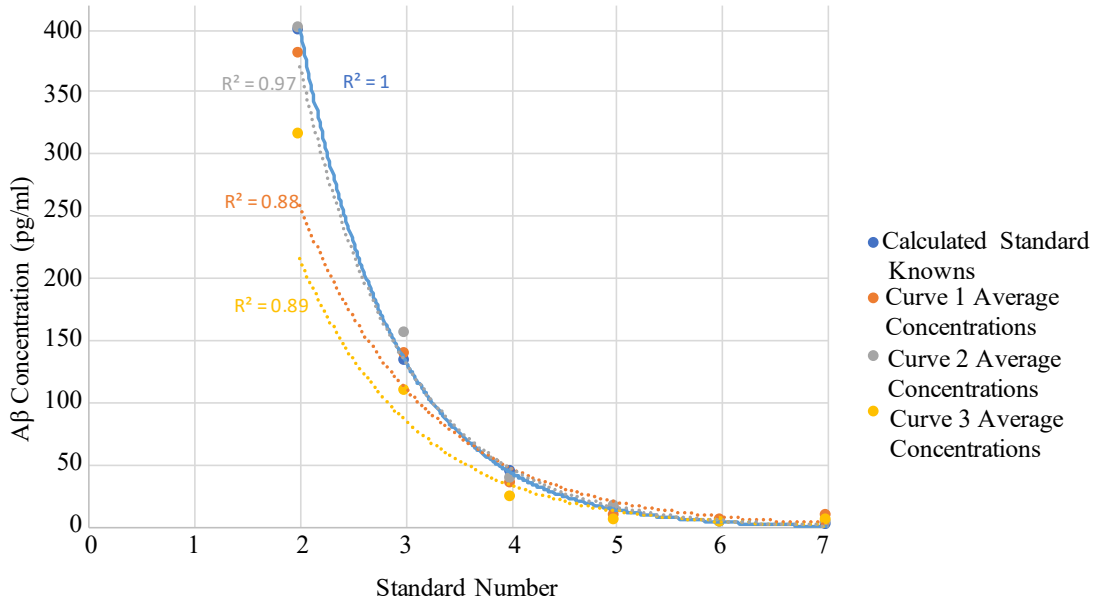

Figure 14: Comparison of Experimental and Calculated Amyloid Standard Concentrations of $A\beta_{40}$ Standard Practice Curves in Triplicate #2
Calculated concentrations of the standard curve were compared to the actual values. Calculated values are shown in blue with a R^2 of 1, while the experimental values are shown in orange for curve 1, grey for curve 2 and yellow for curve 3. R^2 were 0.88, 0.97 and 0.89, respectively. The calculated standard concentrations were as follows: B: 0 pg/ml, S1: 1200 pg/ml, S2: 400 pg/ml, S3: 133.3 pg/ml, S4: 44.4 pg/ml, S5: 14.8 pg/ml, S6: 4.9 pg/ml, and S7: 1.6 pg/ml.

After the BCA was complete, ELISAs were ran on the samples for both $A\beta_{40}$ and $A\beta_{42}$. Both the curve and the samples were loaded in duplicated, and the plate layout is shown in Figure 15. The normalized sample concentrations average for each duplicate pair are documented in Table 10. Within each sample, across all buffers and isoforms, values correspond tightly.

Samples 1, 4 and 6 had low values of both Aβ isoforms within the PBS and triton fractions and no insoluble (guanidine fraction) Aβ in either isoform. Sample 3, 7, 8, and 9 had low values of both isoforms within the PBS and triton fractions; however, there were discrepancies between the isoforms in the guanidine fraction. These samples had no $A\beta_{42}$ concentration for the guanidine value, but showed low levels in the $A\beta_{40}$ isoform. Sample 2 had

Table 8: Practice Mouse Tissue Cerebellum Weights

ELISA: Cerebellum Sections	
Sample ID	Mass (g)
1: WT M5	34.68
2: WT M6	19.02
3: WT M7	21.91
4: WT M8	41.94
6: WT 8117	38.06
7: WT 8104	37.60
8: WT 8100	34.61
9: WT 8099	29.54
5: APP 11141-6	24.90
10: APP 11369-6	3164
11: APP 11373-9	41.50
12: APP 11370-1	34.67
13: APP 10945-5	26.24
14: APP 11094-5	24.56
15: APP 11085-2	31.42
16: APP 11091-8	34.19

low levels across all buffers for both isoforms. Sample 10 had high levels of both isoforms in the PBS fraction, but did not match up between the isoforms for the other two buffers. For $A\beta_{40,}$ all three buffers produced high concentration values; but, for $A\beta_{42}$ the triton value was in the middle of the range, and the guanidine value was 0.00. All other samples (5, and 11-16) had relatively high levels across all buffers for both isoforms. Table 11 shows the averages for both wild type and APP mice, as well as the standard deviation within the groups. All APP averages were higher than WT animals (Table 11). For a clear view on the similarity of

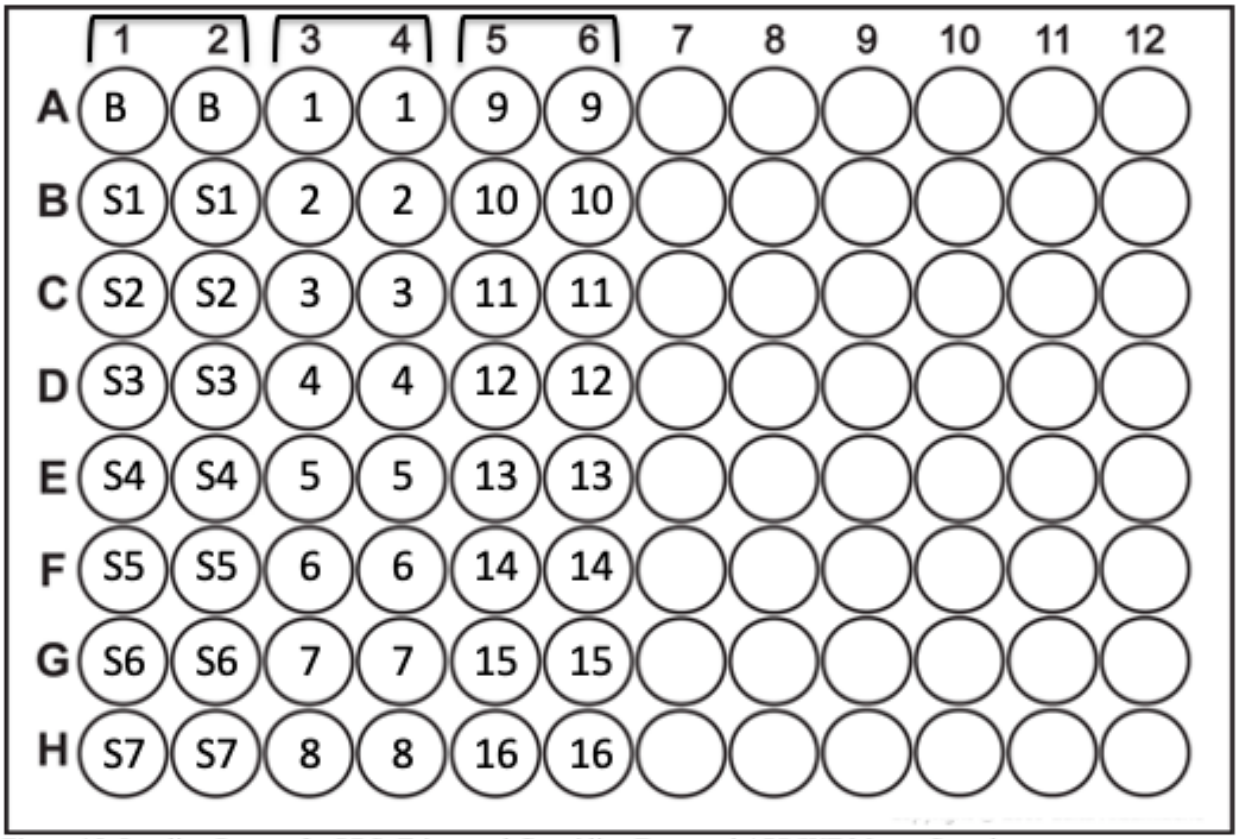

Figure 15: Loading Pattern for PBS, Triton and Guanidine Extracted APP/WT Mouse Samples
Loading pattern of 96-well plate. "S" means standard, and "B" represents blank. The number represents where in the curve the standard falls, with 1 being the beginning of the dilution, and 7 being the final product. The final concentrations of all of the tubes were as followed: For BCA: B- 0 µg/ml, S1- 2500 µg/ml, S2- 125 µg/ml, S3- 62.5 µg/ml, S4- 31.25 µg/ml, S5- 15.625 µg/ml, S6- 7.81 µg/ml, and S7- 3.9µg/ml. For ELISA: B: 0 pg/ml, S1: 1200 pg/ml, S2: 400 pg/ml, S3: 133.3 pg/ml, S4: 44.4 pg/ml, S5: 14.8 pg/ml, S6: 4.9 pg/ml, and S7: 1.6 pg/ml. All samples, including the curve, were loaded in duplicate. Duplicate pairs are indicated by brackets around the lane numbers.

the samples within their respective groups, coefficient of variation (CV) was found (Table 11). Most CV's were fairly low, with the exception of the guanidine fraction for both isoforms in the WT mice. With the exception of the guanidine fractions, WT mice had lower CV between like samples than APP mice.

Citrate Synthase Analysis

Citrate synthase activity within the solei muscles of each mouse were analyzed. Each sample was ran in triplicate, and the average of the three activity values was included in its respective group. Averages for each mouse as well as for each group are depicted in Figure 16. There was no significant difference in enzyme activity between the averages of the sedentary and exercise trained groups.

Table 9: Total Protein Concentrations of APP/WT Mouse Samples

Sample ID	Protein Concentration (mg/ml)		
	PBS	Triton	Guanidine
1: WT M5	2.0	2.1	1.3
2: WT M6	2.9	3.0	2.2
3: WT M7	3.3	2.7	1.9
4: WT M8	3.1	3.7	3.7
6: WT 8117	3.4	3.4	1.6
7: WT 8104	3.1	3.0	2.3
8: WT 8100	3.9	3.6	2.3
9: WT 8099	5.1	3.2	2.3
5: APP 11141-6	3.1	3.6	2.3
10: APP 11369-6	3.1	2.5	2.1
11: APP 11373-9	1.4	3.8	2.7
12: APP 11370-1	1.8	3.1	2.7
13: APP 10945-5	2.4	2.8	2.7
14: APP 11094-5	2.3	2.5	2.4
15: APP 11085-2	3.5	2.8	2.0
16: APP 11091-8	2.8	3.1	2.8

Table 10: APP/WT Mouse Cerebellum Amyloid Concentrations

Sample ID	Amyloid Beta 40 Concentration (pg Aβ per mg/ml)			Amyloid Beta 42 Concentration (pg Aβ per mg/ml)		
	PBS	Triton	Guanidine	PBS	Triton	Guanidine
1: WT M5	286.18	730.72	0.00	621.99	1004.74	0.00
2: WT M6	481.40	885.71	64860	575.03	1308.52	10662.50
3: WT M7	297.94	989.81	50520	493.81	1618.44	0.00
4: WT M8	815.57	1510.22	0.00	873.56	1762.63	0.00
6: WT 8117	538.65	1349.3	0.00	709.77	1373.86	0.00
7: WT 8104	159.83	1493.62	134860	486.02	1830.59	0.00
8: WT 8100	500.93	1500.67	851440	404.57	1463.07	0.00
9: WT 8099	112.41	1281.37	180067.5	56.04	1349.73	0.00
5: APP 11141-6	5543.14	5664.66	4678757.5	12146.66	3610.47	298532.50
10: APP 11369-6	2257.14	4427.41	1690517.5	10248.07	1439.20	0.00
11: APP 11373-9	898.65	4296.33	6299590	10962.71	2863.85	453445.00
12: APP 11370-1	1490.2	4162.67	5559617.5	7636.78	2015.65	494100.00
13: APP 10945-5	84.425	8229.15	6299590	39.6	3105.93	711627.50
14: APP 11094-5	8201.53	7240.29	6299590	12599.18	3965.97	1135235.00
15: APP 11085-2	3322.98	6320.95	3940877.5	12559.32	2582.96	648140.00
16: APP 11091-8	11631.45	7577.84	6299590	12599.18	4107.41	737892.50

Amyloid Beta Analysis

Amyloid levels in the left hippocampus for each sample were analyzed at Washington University by Dr. John Cirrito's lab using an ELISA. After the serial extraction, the guanidine and triton fractions were analyzed for both $A\beta_{40}$ and $A\beta_{42}$ levels.

Within the guanidine fraction of the hippocampus, exercise training significantly decreased the amount of $A\beta_{40}$ ($p = 0.0047$) and $A\beta_{42}$ ($p=0.0024$) for the chronically stressed group (Figure 17 A-B). For the socially housed mice, exercise did not significantly decrease the amount of either hippocampal Aβ isoform compared to the sedentary controls. When comparing values across housing groups, there was no difference in Aβ levels for the exercise groups. However, for the sedentary groups, the socially housed animals have significantly lower $A\beta_{42}$

levels (p= 0.0009). For the triton fraction, there was no significant difference across any combination of groups (Figure 17 C-D).

Table 11: APP/WT Mouse Cerebellum Amyloid Analysis

Genotype	Amyloid-β_{40}			Amyloid-β_{42}		
	PBS	Triton	Guanidine	PBS	Triton	Guanidine
	Average Concentration (pg/mg/ml)					
WT	399.11	1217.68	160218.44	527.60	1463.95	1332.81
APP	4178.69	5989.91	5133516.25	9848.94	2961.43	559871.56
	Standard Deviation between Samples					
WT	230.7	307.6	287094.1	240.4	268.2	3769.8
APP	4013.6	1601.9	1652007.8	4313.9	935.7	336146.8
	Coefficient of Variation between Samples					
WT	0.58	0.25	1.79	0.46	0.18	2.83
APP	0.96	0.27	0.32	0.44	0.32	0.60

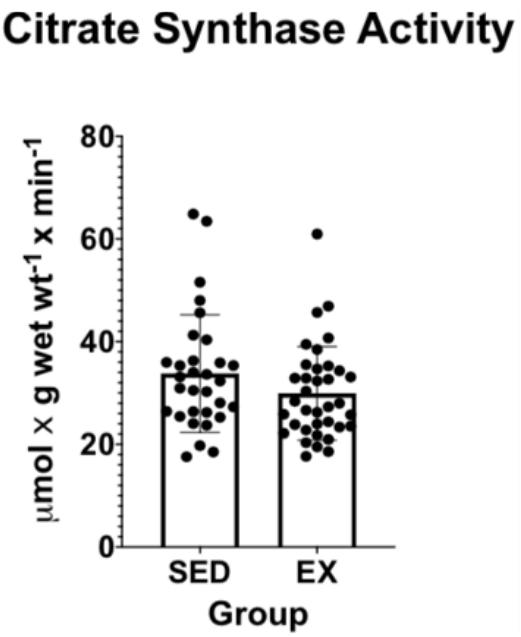

Figure 16. Citrate synthase activity in sedentary and exercised groups.

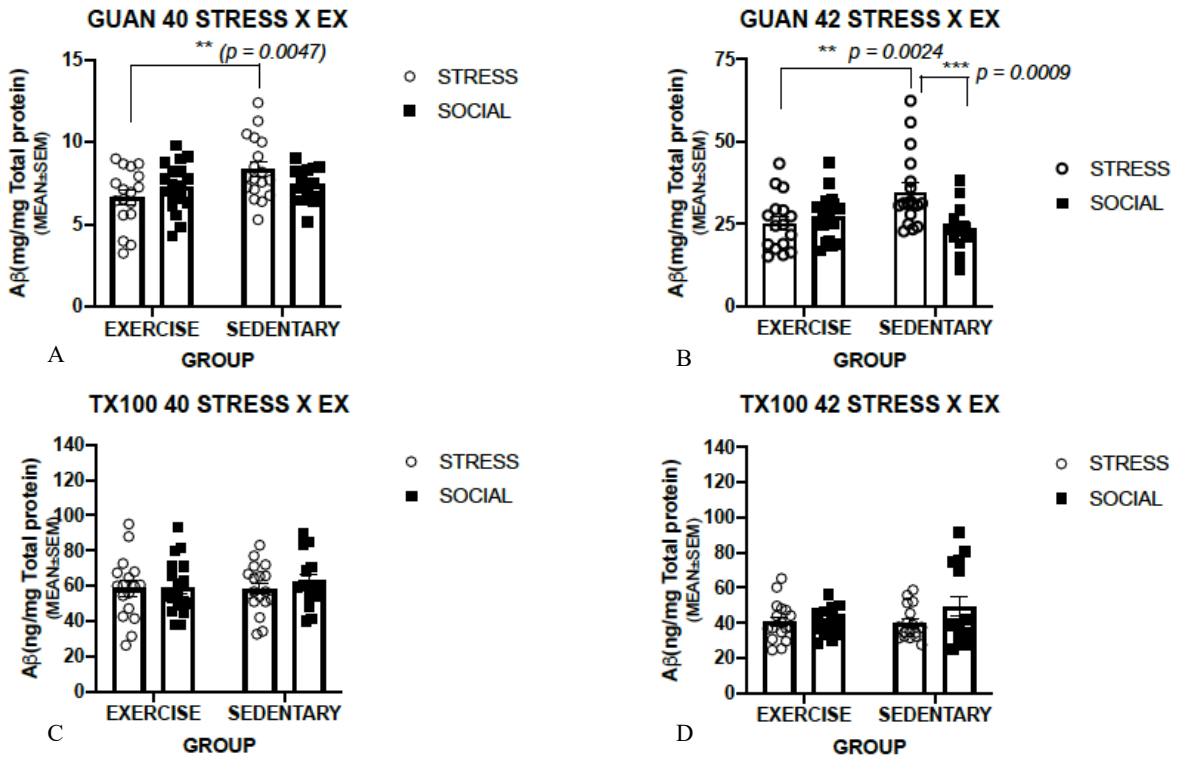

Figure 17. Hippocampal amyloid beta concentrations in social and isolated mice. A) Insoluble $A\beta_{40}$ concentrations. B) Insoluble $A\beta_{42}$ concentrations. C) Soluble $A\beta_{40}$ concentrations. D)Soluble $A\beta_{40}$ concentrations.

DISCUSSION

Standard Curve Practice

Single Practice Curve. Generally, the expected outcome of a decreasing trend was reached (Table 3 and Figure 10), but techniques need additional practice. Standard 1 had to be masked across all duplicate pairs because the value was well above the expected value for the curve (Table 2-3). This is normal for the laboratory, and the aim is to get a 5-6-point curve. This could be corrected by making sure to get the appropriate amount of Aβ to start the curve. While the concentration values for the blanks is noted as <0.00, the absorbance value was slightly higher than the lab's background goal of .01 absorbance. This can be corrected with increased speed, and keeping samples on ice more consistently. Also, standard 5 seems to have a lower than expected concentration throughout all of the duplicate pairs (Table 2). This could be due to improper mixing techniques. One of the data points within standard 6 was an order of magnitude larger than all of the others. This is likely due to improper mixing or contamination from another well when loading. The <0.00 value of standard 7 in the later duplicate pairs is normal as standard 7 has such a small concentration of Aβ it typically has a value similar to the background value. While the variance is not abnormally high, it could definitely be improved by more accurate pipetting and mixing. The experimental curve had a R^2 value of .7843, which is not considered accurate or successful.

Moving forward, the aliquots of Aβ need to be centrifuged to collect sample at the bottom of the tube for more accurate pipetting. Also, once Aβ is added to the formic acid, then the tube needs to be vortexed to properly mix.

Triple Practice Curves I. As none of the three curves plated demonstrated a decreasing trend, the outcome was unexpected (Table 5, Figure 12). It is likely that the reasons for varying and nondecreasing amyloid levels throughout the triplicate groups of each curve is because of an issue with preparing the curve to be loaded (day 2). If the samples did not get mixed well a disproportionate amount of amyloid could be placed into a standard further down the curve. As for curve 2, with hardly any signal, it seems as if very little amyloid was ever added to the curve (Table 4). This could be due to disruption of the amyloid within the sample tube. Centrifuging the tube longer prior to pipetting from it could be used to correct this. All standards exhibited abnormally high standard deviations, indicating inconsistent pipetting when adding Aβ and mixing.

Triple Practice Curves II. As expected, with the exception of standard 7 in curve 1 and 3, a general decrease in concentration is seem within these samples (Table 7 and Figure 14). Background was low and close to typical backgrounds of more experienced lab technicians. Across all curves, standard 1 had to be masked (Table 6). Although this is typical, it could be because too much amyloid is entering the curve due to underwhelming mixing of the formic acid and amyloid beta, or due to antibody concentrations. This reasoning is also supported by the three values of standard 2 that are also over the top of the curve. Overall, Dr. Cirrito believes that formic acids and amyloid should be combined and then vortexed to ensure proper incorporation. Across all curves, standard 6 and 7 seem to be close to the background, which is also normal within the lab. Within each standard, variance is lower than any other set of curves that had been ran, showing improvement. These can be further improved by increasing mixing of the formic acid and amyloid as well. Overall, these three curves turned out well enough to proceed with the project.

WT/APP Practice Mice

All weights are similar to one another, with only one being slightly below the expected range of 20-45 g (Table 8). Overall mouse body masses are not available, so it cannot be determined whether this mouse has a smaller cerebellum due to a smaller overall body size, or whether there was a possible error during dissection. This indicates that the correct tissues were harvested and being analyzed.

For the total protein assay, expected averages are as follows: PBS- 3.8-4.2 mg/ml, Triton- 4.6-5 mg/ml, and Guanidine- 2.8-3.2 mg/ml. The concentrations in Table 9 are mostly lower than the expected; however, given the age (2+ years) and genotype of these mice the decreased total protein is expected, making the result expected. These animals exhibited normal total protein concentrations for their age and genotype, which allowed for normalization of Aβ concentrations between all animals.

Reasonable concentrations of both amyloid isoforms were found with few exceptions. It is expected that WT mice would have small amounts of amyloid, nearing 0 in the guanidine (insoluble) fraction. APP mice should exhibit larger amounts of amyloid and at 2+ years of age, should have large amounts of insoluble amyloid (guanidine fraction). For amyloid beta 40, samples 7, 8, 9, 2 and 3 seem to have surprisingly high guanidine amyloid (Table 10). This could be due to a number of things, including, but not limited to, contamination, or improper blocking. For amyloid beta 42, sample 2 also has an abnormally high guanidine amyloid level, and sample 10 seems to be lacking any guanidine amyloid which is unexpected (Table 10). The discrepancy with sample 2 could be due to contamination or improper blocking, and the discrepancy with sample 10 indicates that the well was missed upon loading samples, or was loaded with too small of a volume. These discrepancies match with notable increases in CV for

those sample groups (Table 11). Overall, the average amyloid values for APP animals are higher than the WT animals (Table 11), which is expected and indicates a successful ELISA run beginning with sequential extraction through the actual ELISA. With the averages, and relatively low CV values (Table 11), this technique is considered mastered, and the protocol is optimized, allowing for confident analysis of Aβ in actual samples.

Citrate Synthase Analysis

As there was no significant difference in citrate synthase activity between the exercise and sedentary group, it does not appear that the exercise regimen resulted in a training effect. This could be due to a multitude of reasons including subthreshold intensity, or lack of proper exercising by the animals. It is unlikely that the planned exercise training regimen (20 m/min, 60 min/day, 5 days/week for 10 weeks) was subthreshold as previous literature has shown an exercise training effect with a shorter, less intense regimen in similarly aged mice (Yuede et al., 2018). Notes taken throughout the treatment for each mouse point to improper execution of the exercise regimen. For some animals, speed was reduced due to inability to maintain running for 60 minutes at 20m/min. Some animals spent prolonged time on the shockers placed at the end of the treadmill, which could lead to increased stress. With a lack of an exercise training effect, it is impossible to reasonably conclude how exercise training may overcome stress in the pathology of AD.

Amyloid Beta Analysis

Although the exercise training regimen was not successful in producing a training effect, the exercise the mice did receive was enough to rescue the effects of chronic stress on

amyloid beta levels in the guanidine fraction. The guanidine fraction is typically used to measure plaque deposition or vesicular levels of amyloid peptides. As these mice were sacrificed at 6 months of age, it is possible for the guanidine fraction to represent both pools of Aβ. Reduction of both Aβ isoforms with exercised for the stressed mice supports past claims that exercise reduces Aβ (Moore et al., 2016). However, contradictory to past research, the exercise treatment did not reduce Aβ levels of socially housed mice. This can be attested to the lack of exercise training that occurred. For $A\beta_{42}$, in the guanidine-extracted fraction, there is a housing effect. Sedentary mice that were housed socially had significantly less $A\beta_{42}$ than chronically isolated mice. This demonstrates that stress can increase amyloid beta, and that this increase can potentially be rescued with increased exercise. To confirm these trends, more research, where a training effect is observed, is necessary. The triton-extracted fraction showed no difference in amyloid levels between any of the groups. This too can be attested to the lack of exercise training the animals received. While the physical activity these mice endured was enough to see comparative benefits between some groups, it is known that exercise is effective to decrease Aβ in a dose-dependent manner (Moore et al., 2016; Thomas et al., 2020). This means that repeating this experiment with stricter guidelines for following the high intensity exercise regimen could yield more conclusive results.

INTENDED METHODS

Due to the onset of the COVID-19 pandemic, the original goals of this experiment had to be severely modified. All research beside completion of the exercise training regimen and tissue collection for mice that had already begun the treatment had to cease with lab and campus wide closures. With the delay of research, many analytes that were of heavy interest originally had to be reevaluated.

Initially, many analytes other than the ones previously discuss were going to be measured to confirm treatment and to investigate the complex relationships between stress, exercise, the serotonergic system and AD pathology. To confirm that the chronic isolation treatment provoked stress as intended, CRF and CRFR1 levels in the cortex and hippocampus were going to be analyzed via western blotting. As a marker of overall brain health, BDNF was also going to be investigated. BDNF can upregulated by physical activity, and therefore could be used to link the exercise training regimen to slowed progression of the AD pathology (Chapman et al., 2013; Thomas et al., 2020).

To assess the serotonergic system under the conditions and treatments explored in this experiment, serotonin and its receptors were going to be measured. As serotonin is a relatively small neurotransmitter that is hard to directly analyze. In order to get an idea of 5HT levels, tryptophan hydrolase, the key enzyme required for 5HT synthesis would have been assayed for via western blotting. Serotonin receptors 4, 6 and 7 were also going to be analyzed due to previous literature linking those receptors to decreases in Aβ via decreased production (Fischer et al., 2016). By knowing these levels more insight about the modulation of AD pathology due

to serotonergic system could be gained, as well as some insight on the influence of exercise training on serotonin levels.

All of these intended tests would have shed additional light on the complex relationships between stress and exercise, and the effects they have on the serotonergic system and AD pathology. However, with the lack of a training effect, results of these test might have been inconclusive as well.

SUMMARY, CONCLUSIONS AND FUTURE DIRECTIONS

This study aimed to identify the effect of an exercise training regimen and isolation stress on serotonin levels in the cortex and the hippocampus, to investigate a possible correlation in serotonin and Aβ levels following treatment, and to explore the relationship between BDNF, CRF and serotonin levels. Due to the lack of an exercise training effect and the delays in research due to COVID-19, none of these goals were achieved. This experiment confirmed past findings such as the effect of stress on Aβ levels (Dong & Csernansky, 2009; Green et al., 2006). Interestingly, this experiment also showed that there is potential for physical activity to be able to rescue the effects stress on Aβ levels.

This experiment should be recreated, with stricter guidelines for following the exercise training regimen. Past research has shown that 15m/min is above the intensity threshold needed to elicit a training effect from APP/PS1 mice (Yuede et al., 2018), so potentially lowering the speed of the treadmills would increase the likelihood of mice to run for the whole treatment. The intended methods for this experiment should be completed after an exercise training effect is found to achieve the goals outlined in this experiment and to illuminate these important relationships.

REFERENCES

Acheson, A., Conover, J.C., Fandl, J.P., DeChiara, T.M., Russell, M., Thadani, A., Squinto, S.P., Yancopoulos, G.D., Lindsay, R.M., 1995. A BDNF autocrine loop in adult sensory neurons prevents cell death. Nature. 374, 450–453.

Adinoff B., Best SE., Ye W., et al., 2010. Adrenocortical and pituitary glucocorticoid feedback in abstinent alcohol-dependent women. Alcoholism: Clinical and Experimental Research. 34(5), 915–924.

Aguirre E., Hoare Z., Streater A., Spector A., Woods B., Hoe J., Orrell M., 2013. Cognitive stimulation therapy (CST) for people with dementia—who benefits most? Int. J. Geriatr. Psychiatry. 28(3), 284-290

Albert MS., DeKosky ST., Dickson D., Dubois B., Feldman HH., Fox N., et al., 2011. The diagnosis of mild cognitive impairment due to Alzheimer's disease: Recommendations from the National Institute on Aging-Alzheimer's Association workgroups on diagnostic guidelines for Alzheimer's disease. Alzheimer's Dement. 7(3), 270-279.

Allinson TM., Parkin ET., Turner AJ., Hooper NM., 2003. ADAMs family members as amyloid precursor protein α-secretases. J Neurosci. 74, 342–352

Almkvist O., Basun H., Wagner SL., Rowe BA., Wahlund LO., Lannfelt L., 1997. Cerebrospinal fluid levels of alpha-secretase-cleaved soluble amyloid precursor protein mirror cognition in a Swedish family with Alzheimer disease and a gene mutation. Arch Neurol. 54(5), 641–644.

Alzheimer's Association, 2019. Alzheimer's disease facts and figures. Retrieved from https://alz.org/media/Documents/alzheimers-facts-and-figures-2019-r.pdf

Ando K., Iijima K.L., Elliott J.I., Kirino Y., Suzuki T., 2001. Phosphorylation-dependent regulation of the interaction of amyloid precursor protein with Fe65 affects the production of β-amyloid. J Biol Chem. 276, 40353–40361.

Arrighi HM., Neumann PJ., Lieberburg IM., Townsend RJ., 2010. Lethality of Alzheimer disease and its impact on nursing home placement. Alzheimer Dis Assoc Disord. 24(1), 90-95.

Azmitia, E. C., 2020. Evolution of serotonin: sunlight to suicide. Handbook of Behavioral Neuroscience. 31, 3-22.

Bedussi, B., van Lier, M.G.J.T.B., Bartstra, J.W., et al., 2015. Clearance from the mouse brain by convection of interstitial fluid towards the ventricular system. Fluids Barriers CNS. 12, 23.

Behan D.P., 1995. Displacement of corticotropin releasing factor from its binding protein as a possible treatment for Alzheimer's disease. Nature. 378, 284–287.

Bennett BD., Denis P., Haniu M., Teplow DB., Kahn S., Louis JC., Citron M., Vassar R., 2000. A furin-like convertase mediates propeptide cleavage of BACE, the Alzheimer's β-secretase. J Biol Chem. 275, 37712–37717.

Bhattacharyya R., Barren C., Kovacs D. M., 2013. Palmitoylation of amyloid precursor protein regulates amyloidogenic processing in lipid rafts. J. Neurosci. 33, 11169–11183.

Bockaert, J., Claeysen, S., Dumuis, A., and Marin, P., 2010. Classification and signaling characteristics of 5-HT receptors. Handbook of the Behavioral Neurobiology of Serotonin. 1, 103–121.

Buckner, R.L., Snyder, A.Z., Shannon, B.J., LaRossa, G., Sachs, R., Fotenos, A.F., Sheline, Y.I., Klunk, W.E., Mathis, C.A., Morris, J.C., and Mintun, M.A., 2005. Molecular, structural, and functional characterization of Alzheimer's disease: evidence for a relationship between default activity, amyloid, and memory. J. Neurosci. 25, 7709–7717.

Campbell S.N., 2015. Impact of CRFR1 ablation on amyloid-beta production and accumulation in a mouse model of Alzheimer's disease. J. Alzheime Dis. 45, 1175–1184.

Capell A, Steiner H, Willem M, Kaiser H, Meyer C, Walter J, Lammich S, Multhaup G, Haass C., 2000. Maturation and pro-peptide cleavage of β-secretase. J Biol Chem. 275, 30849–30854.

Carter CL., Resnick EM., Mallampalli M., Kalbarczyk A., 2012. Sex and gender differences in Alzheimer's disease: Recommendations for future research. J Womens Health 21(10), 1018-23.

Cavalcante P.A.M., Gregnani M.F., Henrique J.S., Ornellas F.H., Araújo R.C., 2017. Aerobic but not resistance exercise can induce inflammatory pathways via toll-like 2 and 4: a systematic review. Sports Med. - Open. 3(42)

Chapman SB., Aslan S., Spence JS., et al., 2013. Shorter term aerobic exercise improves brain, cognition, and cardiovascular fitness in aging. Front Aging Neurosci. 5(75), 75.

Chasseigneaux S., Allinquant B., 2012. Functions of Abeta, sAPPalpha and sAPPbeta: similarities and differences. J Neurochem. 120(Suppl 1), 99–108.

Chen GF., Xu TH., Yan Y., Zhou YR., Jiang Y., Melcher K., Xu HE., 2017. Amyloid beta: structure, biology and structure-based therapeutic development. Acta Pharmacol Sin. 38, 1205–1235.

Chene G., Beiser A., Au R., Preis SR., Wolf PA., Dufouil C., et al., 2015. Gender and incidence of dementia in the Framingham Heart Study from mid-adult life. Alzheimers Dement 11(3), 310-20.

Choi G.E., 2017. Membrane-associated effects of glucocorticoid on BACE1 upregulation and Aβ generation: involvement of lipid raft-mediated CREB activation. J. Neurosci. 37, 8459–8476.

Choy, R. W.-Y., Cheng, Z., & Schekman, R., 2012. Amyloid precursor protein (APP) traffics from the cell surface via endosomes for amyloid β (Aβ) production in the trans-Golgi network. Proceedings of the National Academy of Sciences. 109(30), E2077-E2082.

Chun Y. S., Park Y., Oh H. G., Kim T. W., Yang H. O., Park M. K., et al., 2015b. O-GlcNAcylation promotes non-amyloidogenic processing of amyloid-β protein precursor via inhibition of endocytosis from the plasma membrane. J. Alzheimers Dis. 44, 261–275.

Cirrito J.R., Kang J.E., Lee J., Stewart F.R., Verges D.K., Silverio L.M., et al., 2008. Endocytosis is required for synaptic activity-dependent release of amyloid-beta *in vivo*. Neuron. 58, 42–51.

Clarris HJ., Key B., Beyreuther K., Masters CL., Small DH., 1995. Expression of the amyloid protein precursor of Alzheimer's disease in the developing rat olfactory system. Brain Res. Dev. Brain Res. 88, 87–95.

Costantini C., Ko MH., Jonas MC., Puglielli L., 2007. A reversible form of lysine acetylation in the ER and Golgi lumen controls the molecular stabilization of BACE1. Biochem J. 407, 383–395.

Deane R., Sagare A., Hamm K., Parisi M., Lane S., Finn MB., Holtzman DM., Zlokovic BV., 2008. apoE isoform-specific disruption of amyloid beta peptide clearance from mouse brain. J Clin Invest. 118, 4002–4013.

Dey S., Singh R. H., Dey P. K., 1992. Exercise training: significance of regional alterations in serotonin metabolism of rat brain in relation to antidepressant effect of exercise. Physiol. Behav. 52, 1095–1099.

Dong H., Csernansky J.G., 2009. Effects of stress and stress hormones on amyloid-beta protein and plaque deposition. J. Alzheime Dis. 18, 459–469.

Dries DR., Shah S., Han YH., Yu C., Yu S., Shearman MS., Yu G., 2009. GLU333 of nicastrin directly participates in gamma-secretase activity. J Biol Chem. 284, 29714–29724.

Ehehalt R., Keller P., Haass C., Thiele C., Simons K., 2003. Amyloidogenic processing of the Alzheimer beta-amyloid precursor protein depends on lipid rafts. J. Cell Biol. 160, 113–123.

Esch FS., Keim PS., Beattie EC., Blacher RW., Culwell AR., Oltersdorf T., McClure D., Ward PJ., 1990. Cleavage of amyloid beta peptide during constitutive processing of its precursor. Science. 248, 1122–1124.

Falkevall A., Alikhani N., Bhushan S., Pavlov PF., Busch K., Johnson KA., Eneqvist T., Tjernberg L., Ankarcrona M., Glaser E., 2006. Degradation of the amyloid beta-protein by the novel mitochondrial peptidasome, PreP. J Biol Chem. 281, 29096–29104.

Ferreira-Vieira T. H., Bastos C. P., Pereira G. S., Moreira F. A., Massensini A. R., 2014. A role for the endocannabinoid system in exercise- induced spatial memory enhancement in mice. Hippocampus. 24, 79–88.

Ferris, L.T., Williams, J.S., Shen, C.-L., 2007. The effect of acute exercise on serum brain-derived neurotrophic factor levels and cognitive function. Med. Sci. Sports Exerc. 39, 728–734.

Fisher, J. R., Wallace, C. E., Tripoli, D. L., Sheline, Y. I., & Cirrito, J. R., 2016. Redundant Gs-coupled serotonin receptors regulate amyloid-β metabolism in vivo. Molecular Neurodegeneration. 11(1), 1–12.

Fraering PC., LaVoie MJ., Ye W., Ostaszewski BL., Kimberly WT., Selkoe DJ., Wolfe MS., 2004a. Detergent-dependent dissociation of active γ-secretase reveals an interaction

between Pen-2 and PS1-NTF and offers a model for subunit organization within the complex. Biochemistry. 43, 323–333.

Francis R., McGrath G., Zhang J., Ruddy DA., Sym M., Apfeld J., Nicoll M., Maxwell M., Hai B., Ellis MC., et al., 2002. aph-1 and pen-2 are required for Notch pathway signaling, gamma-secretase cleavage of betaAPP, and presenilin protein accumulation. Dev Cell. 3, 85–97.

Furukawa K., Sopher BL., Rydel RE., Begley JG., Pham DG., Martin GM., Fox M., Mattson MP., 1996. Increased activity-regulating and neuroprotective efficacy of alpha-secretase-derived secreted amyloid precursor protein conferred by a C-terminal heparin-binding domain. J Neurochem. 67(5), 1882–1896.

Gandy S., Czernik A. J., Greengard P., 1988. Phosphorylation of Alzheimer disease amyloid precursor peptide by protein kinase C and Ca^{2+}/calmodulin-dependent protein kinase II. Proc. Natl. Acad. Sci. U S A. 85, 6218–6221.

Glymour MM., Manly JJ., 2008. Lifecourse social conditions and racial and ethnic patterns of cognitive aging. Neuropsychol Rev.18(3), 223-54.

Gouarné C., Groussard C., Gratas-Delamarche A., Delamarche P., Duclos M., 2005. Overnight urinary cortisol and cortisone add insights into adaptation to training. Med. Sci. Sports Exerc. 37, 1157–1167.

Goutte C., Tsunozaki M., Hale VA., Priess JR., 2002. APH-1 is a multipass membrane protein essential for the Notch signaling pathway in *Caenorhabditis elegans* embryos. Proc Natl Acad Sci. 99,775–779.

Gralle M., Oliveira CL., Guerreiro LH., et al., 2006. Solution conformation and heparin-induced dimerization of the full-length extracellular domain of the human amyloid precursor protein. J. Mol. Biol. 357, 493–508.

Green K.N., 2006. Glucocorticoids increase amyloid-beta and tau pathology in a mouse model of Alzheimer's disease. J. Neurosci. 26, 9047–9056.

Greenfield J. P., Tsai J., Gouras G. K., Hai B., Thinakaran G., Checler F., et al., 1999. Endoplasmic reticulum and trans-Golgi network generate distinct populations of Alzheimer β-amyloid peptides. Proc. Natl. Acad. Sci. U S A. 96, 742–747.

Griffith L. S., Mathes M., Schmitz B., 1995. β-amyloid precursor protein is modified with O-linked N-acetylglucosamine. J. Neurosci. Res. 41, 270–278.

Grimm MO., Mett J., Stahlmann CP., Grösgen S., Haupenthal VJ., Blümel T., Hundsdörfer B., Zimmer VC., Mylonas NT., Tanila H., Müller U., Grimm HS., Hartmann T., 2015. APP intracellular domain derived from amyloidogenic β- and γ-secretase cleavage regulates neprilysin expression. Front Aging Neurosci. 7, 77.

Gu Y., Misonou H., Sato T., Dohmae N., Takio K., Ihara Y., 2001. Distinct intramembrane cleavage of the beta-amyloid precursor protein family resembling gamma-secretase-like cleavage of Notch. J Biol Chem. 276, 35235–35238.

Gunduz-Cinar O., Hill M. N., McEwen B. S., Holmes A., 2013. Amygdala FAAH and anandamide: mediating protection and recovery from stress. Trends Pharmacol. Sci. 34, 637–644.

Gurland BJ., Wilder DE., Lantigua R., Stern Y., Chen J., Killeffer EH., et al., 1999. Rates of dementia in three ethnoracial groups. Int J Geriatr Psychiatry. 14(6), 481-93.

Haan MN., Mungas DM., Gonzalez HM., Ortiz TA., Acharya A., Jagust WJ., 2003. Prevalence of dementia in older latinos: The influence of type 2 diabetes mellitus, stroke and genetic factors. J Am Geriatr Soc. 51, 169-77.

Haass C., Hung AY., Schlossmacher MG., Teplow DB., Selkoe DJ., 1993b. Beta-amyloid peptide and a 3-kDa fragment are derived by distinct cellular mechanisms. J Biol Chem. 268, 3021–3024.

Haass C., Kaether C., Thinakaran G., Sisodia S., 2012. Trafficking and proteolytic processing of APP. Cold Spring Harb Perspect Med. 2, a006270.

Haass C., Koo E. H., Mellon A., Hung A. Y., Selkoe D. J., 1992. Targeting of cell-surface β-amyloid precursor protein to lysosomes: alternative processing into amyloid-bearing fragments. Nature. 357, 500–503.

Haniu M., Denis P., Young Y., Mendiaz EA., Fuller J., Hui JO., Bennett BD., Kahn S., Ross S., Burgess T., Katta V., Rogers G., Vassar R., Citron M., 2000. Characterization of Alzheimer's β-secretase protein BACE. A pepsin family member with unusual properties. J Biol Chem. 275, 21099–21106.

He W., Goodkind D., Kowal P., 2016. U.S. Census Bureau, International Population Reports P95/16-1, An Aging World. U.S. Government Publishing Office, Washington, D.C.

Heber S., Herms J., Gajic V., et al., 2000. Mice with combined gene knock-outs reveal essential and partially redundant functions of amyloid precursor protein family members. J. Neurosci. 20, 7951–7963.

Hebert LE., Beckett LA., Scherr PA., Evans DA., 2001. Annual incidence of Alzheimer disease in the United States projected to the years 2000 through 2050. Alzheimer Dis Assoc Disord. 15(4), 169-173.

Hebert LE., Weuve J., Scherr PA., Evans DA., 2013. Alzheimer disease in the United States (2010-2050) estimated using the 2010 Census. Neurology. 80(19), 1778-1783.

Hefter D., Draguhn A., 2017. APP as a protective factor in acute neuronal insults. Front Mol Neurosci. 10, 22.

Heron M., 2018. Deaths: Leading causes for 2016. National Vital Statistics Reports. 67(6)

Hersh LB., 2006. The insulysin (insulin degrading enzyme) enigma. Cell Mol Life Sci. 63, 2432–2434.

Heyman E., Gamelin F. X., Goekint M., Piscitelli F., Roelands B., Leclair E., et al., 2012. Intense exercise increases circulating endocannabinoid and BDNF levels in humans—possible implications for reward and depression. Psychoneuroendocrinology. 37, 844–851.

Hick M., Herrmann U., Weyer SW., Mallm JP., Tschäpe JA., Borgers M., Mercken M., Roth FC., Draguhn A., Slomianka L., Wolfer DP., Korte M., Müller UC., 2015. Acute function of secreted amyloid precursor protein fragment APPsα in synapsis plasticity. Acta Neuropathol. 129, 21–37.

Hill M. N., Titterness A. K., Morrish A. C., Carrier E. J., Lee T. T. Y., Gil- Mohapel J., et al., 2010. Endogenous cannabinoid signaling is required for voluntary exercise-induced enhancement of progenitor cell proliferation in the hippocampus. Hippocampus. 20, 513–523.

Hiltunen M., Lu A., Thomas A. V., Romano D. M., Kim M., Jones P. B., et al., 2006. Ubiquilin 1 modulates amyloid precursor protein trafficking and Aβ secretion. J. Biol. Chem. 281, 32240–32253.

Hitt BD., Jaramillo TC., Chetkovich DM., Vassar R., 2010. BACE1-/- mice exhibit seizure activity that does not correlate with sodium channel level or axonal localization. Mol Neurodegener. 5, 31–34.

Hong L., Koelsch G., Lin X., Wu S., Terzyan S., Ghosh A.K., Zhang X.C., Tang J., 2000. Structure of the protease domain of memapsin 2 (beta-secretase) complexed with inhibitor. Science. 290, 150–153.

Hornsten A., Lieberthal J., Fadia S., Malins R., Ha L., Xu X., Daigle I., Markowitz M., O'Connor G., Plasterk R., Li C., 2007. APL-1, a caenorhabditis elegans protein related to the human beta-amyloid precursor protein, is essential for viability. Proc Natl Acad Sci. 104(6), 1971–1976.

Huang T., Larsen KT., Ried-Larsen M., Møller NC., Andersen LB., 2014. The effects of physical activity and exercise on brain-derived neurotrophic factor in healthy humans: A review. Scand J Med Sci Sports. 24(1), 1-10.

Huang SM., Mouri A., Kokubo H., Nakajima R., Suemoto T., Higuchi M., Staufenbiel M., Noda Y., Yamaguchi H., Nabeshima T., et al., 2006. Neprilysin-sensitive synapse- associated amyloid-b peptide oligomers impair neuronal plasticity and cognitive function. J Biol Chem. 281, 17941 – 17951.

Isohara T., Horiuchi A., Watanabe T., Ando K., Czernik A. J., Uno I., et al., 1999. Phosphorylation of the cytoplasmic domain of Alzheimer's β-amyloid precursor protein at Ser655 by a novel protein kinase. Biochem. Biophys. Res. Commun. 258, 300–305.

Ito S., Ohtsuki S., Terasaki T., 2006. Functional characterization of the brain-to-blood efflux clearance of human amyloid-beta peptide (1-40) across the rat blood-brain barrier. Neurosci Res. 56, 246–252.

Ives DG., Samuel P., Psaty BM., Kuller LH., 2009. Agreement between nosologist and Cardiovascular Health Study review of deaths: Implications of coding differences. J Am Geriatr Soc. 57(1), 133-9.

Iwata N., Mizukami H., Shirotani K., Takaki Y., Muramatsu S., Lu B., et al., 2004. Presynaptic localization of neprilysin contributes to efficient clearance of amyloid-beta peptide in mouse brain. J Neurosci. 24(4), 991–8.

Iwata N., Tsubuki S., Takaki Y., Shirotani K., Lu B., Gerard NP., Gerard C., Hama E., Lee HJ., Saido TC., 2001. Metabolic regulation of brain Abeta by neprilysin. Science. 292, 1550 – 1552.

Jack CR., Albert MS., Knopman DS., McKhann GM., Sperling RA., Carrillo MC., et al., 2011. Introduction to the recommendations from the National Institute on Aging-Alzheimer's Association workgroups on diagnostic guidelines for Alzheimer's disease. Alzheimer's Dement. 7(3), 257-262.

Kamenetz F., Tomita T., Hsieh H., Seabrook G., Borchelt D., Iwatsubo T., Sisodia S., Malinow R., 2003. APP processing and synaptic function. Neuron. 37(6), 925–937.

Kanemitsu H., Tomiyama T., Mori H., 2003. Human neprily- sin is capable of degrading amyloid beta peptide not only in the monomeric form but also the pathological oligo-meric form. Neurosci Lett. 350, 113–116.

Kang J., Lemaire H. G., Unterbeck A., Salbaum J. M., Masters C. L., Grzeschik K. H., et al., 1987. The precursor of Alzheimer's disease amyloid A4 protein resembles a cell-surface receptor. Nature. 325, 733–736.

Khalifa NB., Van Hees J., Tasiaux B., Huysseune S., Smith SO., Constantinescu SN., et al., 2010. What is the role of amyloid precursor protein dimerization? Cell Adhesion & Migration. 4(2), 268–272.

Kienlen-Campard P., Miolet S., Tasiaux B., Octave JN., 2002. Intracellular amyloid-beta1-42, but not extracellular soluble amyloid-beta peptides, induces neuronal apoptosis. J Biol Chem. 277. 15666–15670.

Kim HS., Kim EM., Lee JP., Park CH., Kim S., Seo JH., Chang KA., Yu E., Jeong SJ., Chong YH., Suh YH., 2003. C-terminal fragments of amyloid precursor protein exert neurotoxicity by inducing glycogen synthase kinase-3beta expression. FASEB J. 17, 1951–1953.

Kinoshita A., Fukumoto H., Shah T., Whelan C.M., Irizarry M.C., Hyman B.T., 2003. Demonstration by FRET of BACE interaction with the amyloid precursor protein at the cell surface and in early endosomes. J. Cell Sci. 116, 3339–3346.

Kuhn PH., Wang H., Dislich B., Colombo A., Zeitschel U., Ellwart JW., Kremmer E., Rossner S., Lichtenthaler SF., 2010. ADAM10 is the physiologically relevant, constitutive alpha-secretase of the amyloid precursor protein in primary neurons. EMBO J. 29, 3020–3032.

Kwon OY., Hwang, K., Kim, JA., Kim, K., Kwon, IC., Song, HK., et al., 2010. Dab1 binds to Fe65 and diminishes the effect of Fe65 or LRP1 on APP processing. J Cell Biochem.

Labsy Z., Prieur F., Le Panse B., Do M. C., Gagey O., Lasne F., et al., 2013. The diurnal patterns of cortisol and dehydroepiandrosterone in relation to intense aerobic exercise in recreationally trained soccer players. Stress. 16, 261–265.

Lah, J.J., & Levey, A.I., 2000. Endogenous presenilin-1 targets to endocytic rather than biosynthetic compartments. Mol. Cell. Neurosci. 16, 111–126.

Lai A., Sisodia SS., Trowbridge IS., 1995. Characterization of sorting signals in the beta-amyloid precursor protein cytoplasmic domain. J. Biol. Chem. 270, 3565–3573.

Lannfelt L., Basun H., Wahlund LO., Rowe BA., Wagner SL., 1995. Decreased alpha-secretase-cleaved amyloid precursor protein as a diagnostic marker for Alzheimer's disease. Nat Med. 1(8), 829–832.

Laurin D., Verreault R., Lindsay J., MacPherson K., Rockwood K., 2001. Physical activity and risk of cognitive impairment and dementia in elderly persons. Arch Neurol. 58(3), 498-504.

LaVoie MJ., Fraering PC., Ostaszewski BL., Ye W., Kimberly WT., Wolfe MS., Selkoe DJ., 2003. Assembly of the gamma-secretase complex involves early formation of an intermediate subcomplex of Aph-1 and nicastrin. J Biol Chem. 278, 37213–37222.

Leem YH., Lee YI., Son HJ., Lee SH., 2011. Chronic exercise ameliorates the neuroinflammation in mice carrying NSE/htau23. Biochem Biophys Res Commun. 406, 359–365.

Liao MC., Van Nostrand WE., 2010. Degradation of soluble and fibrillar amyloid b-protein by matrix metallo- proteinase (MT1-MMP) in vitro. Biochemistry. 49, 1127 – 1136.

Lee J.H., Barral S., Reitz C., 2008.The neuronal sortilin-related receptor gene SORL1 and late-onset Alzheimer's disease. Curr Neurol Neurosci Rep. 8, 384–391.

Leissring MA., Farris W., Wu X., Christodoulou DC., Haigis MC., Guarente L., Selkoe DJ., 2004. Alternative translation initiation generates a novel isoform of insulin-degrading enzyme targeted to mitochondria. Biochem J. 383, 439 – 446.

Leissring MA., Farris W., Chang AY., Walsh DM., Wu X., Sun X., Frosch MP., Selkoe DJ., 2003. Enhanced proteolysis of beta-amyloid in APP transgenic mice prevents plaque formation, secondary pathology, and premature death. Neuron. 40, 1087–1093.

Lines LM., Sherif NA., Wiener JM., 2014. Racial and ethnic disparities among individuals with Alzheimer's disease in the United States: A literature review. Research Triangle Park, NC: RTI Press.

Lu B., Nagappan G., Lu Y., 2014. BDNF and synaptic plasticity, cognitive function, and dysfunction. Handb Exp Pharmacol. 220, 223-50.

Machado A., 2014. Chronic stress as a risk factor for Alzheimer's disease. Rev. Neurosci. 25, 785–804.

Magara F., Muller U., Li ZW., Lipp HP., Weissmann C., Stagljar M., Wolfer DP., 1999. Genetic background changes the pattern of forebrain commissure defects in transgenic mice underexpressing the beta-amyloid-precursor protein. Proc. Natl Acad. Sci. USA. 96, 4656–4661.

Mayeda ER., Glymour MM., Quesenberry CP., Whitmer RA., 2016. Inequalities in dementia incidence between six racial and ethnic groups over 14 years. Alzheimers Dement. 12(3), 216-24.

McKhann GM., Knopman DS., Chertkow H., Hyman BT., Jack CR., Kawas CH., et al., 2011. The diagnosis of dementia due to Alzheimer's disease: Recommendations from the National Institute on Aging-Alzheimer's Association workgroups on diagnostic guidelines for Alzheimer's disease. Alzheimer's Dement. 7(3), 263-269.

Meeusen R., De Meirleir K., 1995. Exercise and brain neurotransmission. Sports Med. 20(3), 160-88.

Meilandt WJ., Cisse M., Ho K., Wu T., Esposito LA., Scearce- Levie K., Cheng IH., Yu GQ., Mucke L., 2009. Neprilysin overexpression inhibits plaque formation but fails to reduce pathogenic Abeta oligomers and associated cognitive deficits in human amyloid precursor protein trans- genic mice. J Neurosci. 29, 1977–1986.

Meziane H., Dodart JC., Mathis C., Little S., Clemens J., Paul SM., Ungerer A., 1998. Memory-enhancing effects of secreted forms of the beta-amyloid precursor protein in normal and amnestic mice. Proc Natl Acad Sci. 95(21), 12683–12688.

Mitchell AJ., Shiri-Feshki M., 2009. Rate of progression of mild cognitive impairment to dementia: Meta-analysis of 41 robust inception cohort studies. Acta Psychiatr. Scand. 119, 252-265.

Moore KM., Girens RE., Larson SK., Jones MR., Restivo JL., Holtzman DM., et al., 2016. A spectrum of exercise training reduces soluble Abeta in a dose-dependent manner in a mouse model of Alzheimer's disease. Neurobiol Dis. 85, 218–224.

Morrissey, J. A., Bigus, E., Necarsulmer, J. C., Srinivasan, V., Peppercorn, K., O'Leary, D. J., Abraham, W. C., 2019. The Tripeptide RER Mimics Secreted Amyloid Precursor Protein-Alpha in Upregulating LTP. Frontiers in Cellular Neuroscience.

Muresan V., Muresan Z., 2012. A persistent stress response to impeded axonal transport leads to accumulation of amyloid-β in the endoplasmic reticulum and is a probable cause of sporadic Alzheimer's disease. Neurodegener. Dis. 10, 60–63.

Nalivaeva NN., Turner AJ., 2013. The amyloid precursor protein: A biochemical enigma in brain development, function and disease. FEBS Lett. 587, 2046–2054.

Ng TKS., Ho CSH., Tam WWS., Kua EH., Ho RC., 2019. Decreased Serum Brain-Derived Neurotrophic Factor (BDNF) Levels in Patients with Alzheimer's Disease (AD): A Systematic Review and Meta-Analysis. Int J Mol Sci. 20(2), 257.

Nhan H.S., Chiang K., Koo E.H., 2015. The multifaceted nature of amyloid precursor protein and its proteolytic fragments: friends and foes. Acta Neuropathol. 129 1–19.

Oduah EI., Linhardt RJ., Sharfstein ST., 2016. Heparin: past, present, and future. Pharmaceuticals (Basel). 9(3), E38.

Oishi M., Nairn A. C., Czernik A. J., Lim G. S., Isohara T., Gandy S. E., et al., 1997. The cytoplasmic domain of Alzheimer's amyloid precursor protein is phosphorylated at Thr654, Ser655, and Thr668 in adult rat brain and cultured cells. Mol. Med. 3, 111–123.

Pahlsson P., Shakin-Eshleman S.H., Spitalnik S.L., 1992. N-linked glycosylation of β-amyloid precursor protein. Biochem. Biophys. Res. Commun. 189, 1667–1673.

Park H.J., 2015. The stress response neuropeptide CRF increases amyloid-beta production by regulating gamma-secretase activity. EMBO J. 34, 1674–1686.

Pastorino L., Ikin AF., Nairn AC., Pursnani A., Buxbaum JD., 20012 The carboxylterminus of BACE contains a sorting signal that regulates BACE trafficking but not the formation of total Aβ Mol Cell Neurosci. 19, 175–185.

Patrick, R.P., Ames, B.N., 2015. Vitamin D and the omega-3 fatty acids control serotonin synthesis and action, part 2: relevance for ADHD, bipolar disorder, schizophrenia, and impulsive behavior. The FASEB Journal. 29, 2207-2222.

Pedersen W.A., 2001. Impact of aging on stress-responsive neuroendocrine systems. Mech. Ageing Dev. 122, 963–983.

Plummer S., Van den Heuvel C., Thornton E., Corrigan F., Cappai R., 2016. The neuroprotective properties of the amyloid precursor protein following traumatic brain injury. Aging Dis. 7, 163–179.

Potter GG., Plassman BL., Burke JR., Kabeto MU., Langa KM., Llewellyn DJ., et al., 2009. Cognitive performance and informant reports in the diagnosis of cognitive impairment and dementia in African Americans and whites. Alzheimers Dement. 5(6), 445-53.

Prokop S., Shirotani K., Edbauer D., Haass C., Steiner H., 2004. Requirement of PEN-2 for stabilization of the presenilin N-/C-terminal fragment heterodimer within the gamma-secretase complex. J Biol Chem. 279, 23255–23261.

Radak, Z., Ihasz, F., Koltai, E., Goto, S., Taylor, A.W., Boldogh, I., 2014. The redox-associated adaptive response of brain to physical exercise. Free Radic. Res. 48, 84–92.

Rajan KB., Weuve J., Barnes LL., Wilson RS., Evans DA., 2019. Prevalence and incidence of clinically diagnosed Alzheimer's disease dementia from 1994 to 2012 in a population study. Alzheimers Dement. 15(1)

Ranabir S., Reetu K., 2011. Stress and hormones. Indian J Endocrinol Metab. 15(1), 18-22.

Rehman H.U., 2002. Role of CRH in the pathogenesis of dementia of Alzheimer's type and other dementias. Curr. Opin. Invest. Drugs. 3, 1637–1642.

Reich C. G., Taylor M. E., McCarthy M. M., 2009. Differential effects of chronic unpredictable stress on hippocampal CB1 receptors in male and female rats. Behav. Brain Res. 203, 264–269.

Ring S., Weyer SW., Kilian SB., Waldron E., Pietrzik CU., Filippov MA., Herms J., Buchholz C., Eckman CB., Korte M., Wolfer DP., Muller UC., 2007. The secreted beta-amyloid precursor protein ectodomain APPs alpha is sufficient to rescue the anatomical, behavioral, and electrophysiological abnormalities of APP-deficient mice. J Neurosci. 27(29), 7817–7826.

Roberts R., Knopman DS., 2013. Classification and epidemiology of MCI. Clin Geriatr Med. 29(4), 753-72.

Roch JM., Masliah E., Roch-Levecq AC., Sundsmo MP., Otero DA., Veinbergs I., Saitoh T., 1994. Increase of synaptic density and memory retention by a peptide representing the

trophic domain of the amyloid beta/A4 protein precursor. Proc Natl Acad Sci. 91(16), 7450–7454.

Rohan de Silva HA., Jen A., Wickenden C., Jen LS., Wilkinson SL., Patel AJ., 1997. Cell-specific expression of beta-amyloid precursor protein isoform mRNAs and proteins in neurons and astrocytes. Brain Res. Mol. Brain Res. 47, 147–156.

Rohe M., Synowitz M., Glass R., Paul S.M., Nykjaer A., Willnow T.E., 2009. Brain-derived neurotrophic factor reduces amyloidogenic processing through control of SORLA gene expression. J Neurosci. 29, 15472–15478.

Romero JP., Benito-Leon J., Mitchell AJ., Trincado R., Bermejo- Pareja F., 2014. Under reporting of dementia deaths on death certificates using data from a population-based study (NEDICES). J Alzheimers Dis. 39(4), 741-8.

Rossjohn J., Cappai R., Feil SC., et al., 1999. Crystal structure of the N-terminal, growth factor-like domain of Alzheimer amyloid precursor protein. Nat. Struct. Biol. 6, 327–331.

Sabo S.L., Lanier L.M., Ikin A.F., Khorkova O., Sahasrabudhe S., Greengard P., et al., 1999. Regulation of β-amyloid secretion by FE65, an amyloid protein precursor-binding protein. J Biol Chem. 274, 7952–7957.

Saito T., Takaki Y., Iwata N., Trojanowski J., Saido TC., 2006. Alzheimer's disease, neuropeptides, neuropeptidase, amyloid-beta peptide metabolism. Sci Aging Knowledge Environ. PE1.

Salbaum JM., Weidemann A., Lemaire HG., Masters CL., Beyreuther K., 1988. The promoter of Alzheimer's disease amyloid A4 precursor gene. EMBO J. 7, 2807–2813.

Salvagioni D.A.J., 2017. Physical, psychological and occupational consequences of job burnout: a systematic review of prospective studies. PLoS One. 12, e0185781.

Samper-Ternent R., Kuo YF., Ray LA., Ottenbacher KJ., Markides KS., Al Snih S., 2012. Prevalence of health conditions and predictors of mortality in oldest old Mexican Americans and non-Hispanic whites. J Am Med Dir Assn.13(3), 254-9.

Sastre M., Turner R.S., Levy E., 1998. X11 interaction with beta-amyloid precursor protein modulates its cellular stabilization and reduces amyloid β-protein secretion. J Biol Chem. 273, 22351–22357.

Selkoe DJ., Hardy J., 2016. The amyloid hypothesis of Alzheimer's disease at 25 years. EMBO Mol Med. 8, 595–608.

Selkoe DJ., 2001. Alzheimer's disease: genes, proteins, and therapy. Physiol. Rev. 81, 741–766.

Seshadri S., Wolf PA., Beiser A., Au R., McNulty K., White R., et al., 1997. Lifetime risk of dementia and Alzheimer's disease. The impact of mortality on risk estimates in the Framingham Study. Neurology. 49(6), 1498-504.

Seubert P., Vigo-Pelfrey C., Esch F., Lee M., Dovey H., Davis D., Sinha S., Schlossmacher M., Whaley J., Swindlehurst C., et al., 1992. Isolation and quantification of soluble Alzheimer's beta-peptide from biological fluids. Nature. 359, 325–327.

Shah S., Lee SF., Tabuchi K., Hao YH., Yu C., LaPlant Q., Ball H., Dann CE 3rd., Sudhof T., Yu G., 2005. Nicastrin functions as a gamma-secretase-substrate receptor. Cell. 122, 435–447.

Shankar GM., Li S., Mehta TH., Garcia-Munoz A., Shepardson NE., Smith I., Brett FM., Farrell MA., Rowan MJ., Lemere CA., Regan CM., Walsh DM., Sabatini BL., Selkoe DJ., 2008. Amyloid-beta protein dimers isolated directly from Alzheimer's brains impair synaptic plasticity and memory. Nat Med. 14(8), 837–842.

Shen Y., Joachimiak A., Rosner MR., Tang W-J., 2006. Structures of human insulin-degrading enzyme reveal a new substrate mechanism. Nature. 443, 870–874.

Sisodia SS., 1992. Beta-amyloid precursor protein cleavage by a membrane-bound protease. Proc. Natl. Acad. Sci. 89, 6075–6079.

Skovronsky D. M., Moore D. B., Milla M. E., Doms R. W., Lee V. M., 2000. Protein kinase C-dependent α-secretase competes with β-secretase for cleavage of amyloid-β precursor protein in the trans-golgi network. J. Biol. Chem. 275, 2568–2575.

Small DH., Nurcombe V., Reed G., Clarris H., Moir R., Beyreuther K., Masters CL., 1994. A heparin-binding domain in the amyloid protein precursor of Alzheimer's disease is involved in the regulation of neurite outgrowth. J. Neurosci. 14, 2117–2127.

Small S.A., Gandy S., 2006. Sorting through the cell biology of Alzheimer's disease: intracellular pathways to pathogenesis. Neuron. 52, 15–31.

Spasic D., Tolia A., Dillen K., Baert V., De Strooper B., Vrijens S., Annaert W., 2006. Presenilin-1 maintains a nine-transmembrane topology throughout the secretory pathway. J Biol Chem. 281, 26569–26577.

Steiner H., Fluhrer R., Haass C., 2008. Intramembrane proteolysis by gamma-secretase. J Biol Chem. 283, 29627–29631.

Stephens MA., Wand G., 2012. Stress and the HPA axis: role of glucocorticoids in alcohol dependence. Alcohol Res. 34(4), 468-483.

Storck, S.E., Meister, S., Nahrath, J., Meißner, J.N., Schubert, N., Spiezio, A. Di, Pietrzik, C.U., 2016. Endothelial LRP1 transports amyloid-β1–42 across the blood-brain barrier. The Journal of Clinical Investigation. 126(1), 123–136.

Sutoo D., Akiyama K., 2003. Regulation of brain function by exercise. Neurobiol Dis. 13(1), 1-14.

Suzuki T., Nairn A. C., Gandy S. E., Greengard P., 1992. Phosphorylation of Alzheimer amyloid precursor protein by protein kinase C. Neuroscience. 48, 755–761.

Taylor CJ., Ireland DR., Ballagh I., Bourne K., Marechal NM., Turner PR., Bilkey DK., Tate WP., Abraham WC., 2008. Endogenous secreted amyloid precursor protein-alpha regulates hippocampal NMDA receptor function, long-term potentiation and spatial memory. Neurobiology Dis. 31(2), 250–260.

Thathiah A., De Strooper B., 2011. The role of G protein-coupled receptors in the pathology of Alzheimer's disease. Nat. Rev. Neurosci. 12, 73–87.

Thomas, R., Zimmerman, S. D., Yuede, K. M., Cirrito, J. R., Tai, L. M., Timson, B. F., Yuede, C. M., 2020. Exercise training results in lower amyloid plaque load and greater cognitive function in an intensity dependent manner in the tg2576 mouse model of Alzheimer's disease. Brain Sciences. 10(2), 88.

Thornton E., Vink R., Blumbergs PC., Van Den Heuvel C., 2006. Soluble amyloid precursor protein alpha reduces neuronal injury and improves functional outcome following diffuse traumatic brain injury in rats. Brain Res. 1094(1), 38–46.

Turner AJ., Isaac RE., Coates D., 2001. The neprilysin (NEP) family of zinc metalloendopeptidases: Genomics and function. Bioessays. 23, 261–269.

Tsatsoulis A., Fountoulakis S., 2006. The protective role of exercise on stress system dysregulation and comorbidities. Ann N Y Acad Sci. 1083, 196-213.

Ulrich-Lai YM., Herman JP., 2009. Neural regulation of endocrine and autonomic stress responses. Nat Rev Neurosci. 10(6), 397-409.

U.S. Census Bureau., 2014. National Population Projections: Downloadable Files. Available at: https://www.census.gov/data/ datasets/2014/demo/popproj/2014-popproj.html.

U.S. Department of Health and Human Services, Centers for Disease Control and Prevention, National Center for Health Statistics., 2017. CDC WONDER online database: About Underlying Cause of Death, 1999-2017. Available at: http://wonder.cdc. gov/ucd-icd10.html.

Vetrivel KS., Meckler X., Chen Y., Nguyen PD., Seidah NG., Vassar R., Wong PC., Fukata M., Kounnas MZ., Thinakaran G., 2009. Alzheimer disease Aβ production in the absence of S-palmitoylation-dependent targeting of BACE1 to lipid rafts. J Biol Chem. 284, 3793–3803.

Wang X., Zhou X., Li G., Zhang Y., Wu Y., Song W., 2017. Modifications and trafficking of APP in the pathogenesis of Alzheimer's disease. Front Mol Neurosci. 10, 294

Wang Y., Ha Y., 2004. The X-ray structure of an antiparallel dimer of the human amyloid precursor protein E2 domain. Mol Cell. 15, 343–353.

Wasco W., Gurubhagavatula S., Paradis MD., Romano DM., Sisodia SS., Hyman BT., Neve RL., Tanzi RE., 1993. Isolation and characterization of APLP2 encoding a homologue of the Alzheimer's associated amyloid beta protein precursor. Nat Genet. 5, 95–100.

Watanabe T., Hikichi Y., Willuweit A., Shintani Y., Horiguchi T., 2012. FBL2 regulates amyloid precursor protein (APP) metabolism by promoting ubiquitination-dependent APP degradation and inhibition of APP endocytosis. J. Neurosci. 32, 3352–3365.

Weuve J., Hebert LE., Scherr PA., Evans DA, 2015.. Prevalence of Alzheimer disease in U.S. states. Epidemiology. 26(1), E4-6.

Weyer SW., Klevanski M., Delekate A., Voikar V., Aydin D., Hick M., Filippov M., Drost N., Schaller KL., Saar M., Vogt MA., Gass P., Samanta A., Jaschke A., Korte M., Wolfer DP., Caldwell JH., Muller UC., 2011. APP and APLP2 are essential at PNS and CNS synapses for transmission, spatial learning and LTP. Embo J. 30, 2266–2280.

Willem M., 2015. eta-Secretase processing of APP inhibits neuronal activity in the hippocampus. Nature. 526, 443–447.

Willem M., Garratt AN., Novak B., Citron M., Kaufmann S., Rittger A., DeStrooper B., Saftig P., Birchmeier C., Haass C., 2006. Control of peripheral nerve myelination by the β-secretase BACE1. Science. 314, 664–666.

Wilson R.S., 2006. Chronic psychological distress and risk of Alzheimer's disease in old age. Neuroepidemiology. 27, 143–153.

Wilson, R.S., Barnes, L.L., Bennett, D.A., Li, Y., Bienias, J.L., Mendes de Leon, C.F., and Evans, D.A., 2005. Proneness to psychological distress and risk of Alzheimer disease in a biracial community. Neurology. 64, 380–382.

Wilson R.S., 2003. Proneness to psychological distress is associated with risk of Alzheimer's disease. Neurology. 61, 1479–1485.

Wilson RS., Bennett DA., Bienias JL., Aggarwal NT., Mendes De Leon CF., Morris MC., Schneider JA., Evans DA., 2002. Cognitive activity and incident AD in a population-based sample of older persons. Neurology. 59(12), 1910-4.

Wolfe MS., Kopan R., 2004. Intramembrane proteolysis: Theme and variations. Science. 305, 1119–1123

Wolfe MS., Xia W., Ostaszewski BL., Diehl TS., Kimberly WT., Selkoe DJ., 1999. Two transmembrane aspartates in presenilin-1 required for presenilin endoproteolysis and gamma-secretase activity. Nature. 398, 513–517.

Wüst S., Wolf J., Hellhammer D. H., Federenko I., Schommer N., Kirschbaum C., 2000. The cortisol awakening response—normal values and confounds. Noise Health. 2, 79.

Xue Y., Lee S., Wang Y., Ha Y., 2011. Crystal structure of the E2 domain of amyloid precursor protein-like protein 1 in complex with sucrose octasulfate. J. Biol. Chem. 286, 29748–29757.

Yamazaki T., Koo EH., Selkoe DJ., 1996. Trafficking of cell-surface amyloid beta-protein precursor. II. Endocytosis, recycling and lysosomal targeting detected by immunolocalization. J. Cell Sci.109, 999–1008.

Yan P., Hu X., Song H., Yin K., Bateman RJ., Cirrito JR., Xiao Q., Hsu FF., Turk JW., Xu J., et al., 2006. Matrix metal- loproteinase-9 degrades amyloid-b fibrils in vitro and compact plaques in situ. J Biol Chem. 281, 24566– 24574.

Yan Y., Dominguez S., Fisher DW., Dong H., 2018. Sex differences in chronic stress response and Alzheimer's disease. Neurobiol Stress. 8, 120–6.

Yin KJ., Cirrito JR., Yan P., Hu X., Xiao Q., Pan X., Bateman R., Song H.., Hsu FF, Turk J., et al., 2006. Matrix metallopro- teinases expressed by astrocytes mediate extracellular amyloid-beta peptide catabolism. J Neurosci. 26, 10939– 10948.

Yoshikai S., Sasaki H., Doh-ura K., Furuya H., Sakaki Y., 1990. Genomic organization of the human amyloid β-protein precursor gene. Gene. 87, 257–263.

Yu G., Nishimura M., Arawaka S., Levitan D., Zhang L., Tandon A., Song YQ., Rogaeva E., Chen F., Kawarai T., et al., 2000. Nicastrin modulates presenilin-mediated notch/glp-1 signal transduction and betaAPP processing. Nature. 407, 48–54.

Yuede CM., Timson BF., Hettinger JC., et al., 2018. Interactions between stress and physical activity on Alzheimer's disease pathology. Neurobiol Stress. 8, 158-171.

Yuede C.M., Zimmerman S.D., Dong H., Kling M.J., Bero A.W., Holtzman D.M., Timson B.F., Csernansky J.G., 2009. Effects of voluntary and forced exercise on plaque deposition, hippocampal volume, and behavior in the Tg2576 mouse model of Alzheimer's disease. Neurobiol. Dis. 35, 426–432.

Zambrano N., Bruni P., Minopoli G., Mosca R., Molino D., Russo C., et al., 2001. The β-amyloid precursor protein APP is tyrosine-phosphorylated in cells expressing a constitutively active form of the Abl protoncogene. J. Biol. Chem. 276, 19787–19792.

Zhang Z., Hayward MD., Yu YL., 2016. Life Course Pathways to racial disparities in cognitive impairment among older Americans. J. Health Soc. Behav. 57(2), 184-99.

Zheng H., Jiang M., Trumbauer ME., et al., 1995. beta-Amyloid precursor protein-deficient mice show reactive gliosis and decreased locomotor activity. Cell. 81, 525–531.

Zigmond MJ., Cameron JL., Hoffer BJ., Smeyne RJ., 2012. Neurorestoration by physical exercise: moving forward. Parkinsonism Relat Disord. 18(Suppl 1), S147-50.

APPENDIX

From: Institutional Animal Care and Use Committee (IACUC) <iacuc_no_reply@missouristate.cayuse424.com>
Date: Tuesday, March 5, 2019 at 2:30 PM
To: Zimmerman, Scott D <ScottZimmerman@MissouriState.edu>, Zimmerman, Scott D <ScottZimmerman@MissouriState.edu>
Subject: Application to Use Live Vertebrate Animals

Project Title: **APP/PS1 Mouse Breeding Protocol**
IACUC ID: **19-010.0**
Species: **Mouse**

The above-referenced Application has been approved and the approval can be viewed at:

https://missouristate.cayuse424.com/acap/

If you have any questions, please do not hesitate to contact the Missouri State Office of Research Compliance at iacuc@missouristate.edu or 417-836-8405.

2019-1 IACUC

PJ

Proctor, Janene A Wednesday, February 20, 2019 at 1:32 PM
To: Zimmerman, Scott D; **Cc:** Curry, Bailey J; Timson, Benjamin F; Holtmann, Lydia M

Hello all.

IACUC protocol 2019-1 is approved but it won't move through the system.
I apologize on behalf of the Cayuse system. Please don't do anymore in the new Cayuse. Use the old one if you need to submit a new protocol.

Thank you.

Janene

Janene Proctor
Missouri State University / Office of Research Administration
901 S. National / Carrington 405
Springfield, MO 65897
Phone: 417-836-8419
janeneproctor@missouristate.edu I ora.missouristate.edu